



Synthesis of Nano-silica Oxide for Heavy Metal Decontamination from Aqueous Solutions

Naira Meky · Eslam Salama ·
Mohamed F. Soliman · Soheair G. Naeem ·
Mona Ossman · Mahmoud Elsayed

Received: 8 August 2023 / Accepted: 19 January 2024 / Published online: 14 February 2024
© The Author(s) 2024

Abstract In the current study, nano-silica oxide (nano-SiO₂) was fabricated via the sol-gel technique. Then, the prepared nano-SiO₂ was characterized using X-ray diffractometer (XRD), transmission electron microscopy (TEM) coupled with energy-dispersive X-ray spectroscopy (EDS), Fourier transform infrared spectroscopy (FTIR), thermogravimetric analysis (TGA), and Brunauer-Emmett-Teller (BET) specific surface area analysis. Furthermore, the fabricated nano-SiO₂ was applied for the adsorption of lead Pb (II) and chromium Cr (VI) from aqueous solutions. Additionally, the influence of different operating factors such as contact time (0–180 min), initial pH (1–11), nano-SiO₂ dose (0.1–8 g L⁻¹), initial metal ion concentration (5–100 mg L⁻¹), and the temperature (30–85 °C) was investigated. The nano-SiO₂ doses of 0.5 and 1 g L⁻¹ were selected as the optimal adsorbent dose for the removal of Pb (II) and Cr (VI), respectively. These doses achieved a removal efficiency of 82.3% and 78.5% for Pb (II) and Cr (VI), after 60 and 90 min, at initial pH values of 5 and 2,

respectively, using 10 mg L⁻¹ initial metal concentration, and at room temperature. Lastly, kinetic and equilibrium studies were competently fitted using the pseudo-second-order and Freundlich models, respectively. Adsorption thermodynamic studies designate the spontaneous and thermodynamic nature of the adsorption process. These results reveal the efficiency of the fabricated nano-SiO₂ as an adsorbent for heavy metal removal from aqueous solutions.

Keywords Silica-based nanoparticles · Adsorption · Heavy metal removal · Operating parameters · Optimization · Kinetics · Isotherm · Thermodynamics

1 Introduction

With the expansion of the economy and industry, various heavy metals are surely released into the water through the effluent runoffs of several industries including fertilizers, steel, dyes, batteries, mining, textiles, leather, alloying, electroplating, tannery, paper, food, and cosmetics, causing environmental water pollution (Wadhawan et al., 2020). This leads to the accumulation of heavy metal ions which are non-biodegradable and can enter the human bodies via the feed chain and then immediately threaten human health if they surpass the standard range, due to their high toxicity, carcinogenicity, and biorecalcitrance (Anjum et al., 2023), which makes it mandatory to efficiently remove toxic heavy metals from water.

N. Meky (✉) · M. F. Soliman · S. G. Naeem · M. Elsayed
Civil Engineering Department, Faculty of Engineering,
Aswan University, Aswan 81542, Egypt
e-mail: naira.dawi@aswu.edu.eg; naira.meky@ejust.edu.eg

E. Salama · M. Ossman
Environment and Natural Materials Research Institute
(ENMRI), City of Scientific Research and Technological
Applications (SRTA-City), New Borg El-Arab City,
Alexandria 21934, Egypt

Various conventional techniques are used to eliminate heavy metal ions from water including membrane separation, solvent extraction, chemical precipitation, adsorption, ion exchange, and reverse osmosis (Ammar et al., 2021). Although the aforementioned approaches are effective and meet the discharge limits, most of them still produce secondary waste. Adsorption was compared to various water treatment technologies, and it was found to be more cost-effective than evaporation, aerobic digestion, anaerobic digestion, ion exchange, electrodialysis, reverse osmosis, precipitation, and oxidation (Santhosh et al., 2016).

Consequently, adsorption is regarded as a viable alternative for the removal of hazardous heavy metals from water, due to its accessibility, flexibility, and excellent proficiency (Hasanzadeh et al., 2017). A great perspective for the removal of heavy metals from contaminated water is revealed from the adsorption on the surface of solid adsorbents (Alterary et al., 2022). Due to its simple design, inexpensive initial investment, and minimal area requirement, it is more advantageous than other methods (Cataldo et al., 2016). As a result of these qualities, the adsorption process is gaining great interest from researchers in the treatment of water contaminated with heavy metals (Aragaw & Ayalew, 2023).

To name a few, activated carbon, metal oxides, and clay are some of the main conventional adsorbents applied for the removal of heavy metals (Fathy et al., 2020). These traditional adsorbents have limitations in terms of their reusability, recyclability, and adsorption capabilities (Tu et al., 2017). To overcome these drawbacks, novel adsorbent materials in nanosizes are fabricated and utilized for water decontamination (Maryam & Gul, 2023).

Presently, nanoparticles (NPs) have drawn significant attention as adsorbents for water decontamination, due to their huge specific surface area, low flocculent generation, and availability of many active groups for the binding of heavy metal ions (Verma et al., 2017a). Additionally, they can be recycled and reused repeatedly, which makes them both economical and highly desirable (Verma et al., 2017a, b).

A variety of NP types, including chitosan, carbonaceous, metallic, bimetallic, metal oxide, polymer-based, ferrite, magnetic, and zeolite, have been investigated in previous years for heavy metal removal from water (Karami, 2013). These NPs eliminate the

heavy metals by adsorbing them on their surfaces (Iconaru et al., 2016). Among the above-mentioned NPs that are demonstrated in scientific investigations are silica-based NPs. It is a type of metal oxide NPs that owns a significant deal of promise for adsorbing heavy metal ions, due to their distinctive qualities, including a large surface area, controllable surface characteristics, and clearly defined pore size. Moreover, nano-silica-based materials provide an eco-friendly and non-toxic adsorbent (Li et al., 2019). Different types of silica-based NPs have been investigated by many researchers for the removal of heavy metal removal from water and resulted in boosted adsorption capacity and selectivity. Li et al. (2019) examined the nitrilotriacetic acid-silica gel (NTA-silica gel) for the effective removal of Pb (II), Cd (II), and Cu (II), and Kotsyuda et al. (Kotsyuda et al., 2017) examined amino-functionalized silica NPs for Cu (II) ion removal, and they found that silica-based NPs were very efficient for heavy metal removal with high adsorption capacity. Additionally, Najafi et al. (Najafi et al., 2012) also shed light on the elimination of Pb (II), Cd (II), and Ni (II) using four different silica-based NPs: amino-functionalized nano-silica hollow spheres, nano-silica spheres, non-functionalized, and amino-functionalized nano-silica gel, and found that functionalized nano-silica was more effective than other examined silica-based NPs with maximum adsorption capacities.

The main operational conditions such as initial pH value, adsorbent dose, contact time, temperature, and initial pollutant concentration substantially affect the efficiency of the adsorption process, as reported by many scientific investigations (Kim et al., 2013; Zhang et al., 2022). Therefore, optimal conditions operational are worthy of attention. However, from the literature review, we can conclude that there are no specific favorable operating conditions for heavy metal removal using NPs, as it differs by using different NPs and pollutants. Consequently, to study the influence of each parameter; a wide range must be investigated within the same operating circumstances of the adsorption experiment, and according to the resulting removal observations, the optimum values can be highlighted.

To the best of our knowledge, previous studies have tested mainly the synthesis of silica oxide NPs (nano-SiO₂) using different techniques, without assessing their performance for heavy metal

removal. Additionally, there is a lack of knowledge of the impact of important operating parameters (e.g., initial pH, dosage, temperature, and contact time) on the adsorption of heavy metals using nano-SiO₂. Furthermore, studies have investigated the functionalization of silica-based NPs such as nano-silica functionalized with diethanolamine (Xiong et al., 2019), amino-immobilized nano-silica sorbents (Mahmoud & Al-Bishri, 2011), and nano-silica@follic acid nanocomposite (Mahmoud et al., 2019). It is therefore critical to investigate the adsorption performance of nano-SiO₂ for commonly found metals in environmental matrices (i.e., Pb (II) and Cr (VI)) and the effect of different environmental parameters on the process.

Therefore, in this study, silica oxide nanoparticles (nano-SiO₂) were synthesized, characterized, and applied as an adsorbent material for heavy metal removal from aqueous solutions. More specifically, the main objectives are to use batch experiments to (1) investigate physicochemical characteristics of the synthesized nano-SiO₂ and identify the mechanism of metal removal by the sorbent; (2) assess and compare the adsorption performance of nano-SiO₂ for removal of two common metals found in contaminated water (i.e., Pb (II) and Cr (VI)); (3) study the effect of different operational conditions on metal adsorption, such as contact time (0–180 min), initial pH (1–11), synthesized nano-SiO₂ dosage (0.1–8 g L⁻¹), initial heavy metal concentration (5–100 mg L⁻¹), and solution temperature (average room temperature 30–85 °C); and (4) investigate the thermodynamics, kinetics, and isotherms of the adsorption process.

2 Materials and Methods

2.1 Materials

Tetraethyl orthosilicate (99.9% Alfa Aesar, UK), acetic acid (Sigma-Aldrich), polyvinylpyrrolidone (PVP) (Sigma-Aldrich), and absolute ethanol (99.8%, Acros Organics) have been used for the preparation of the nano-SiO₂. Other chemicals utilized in this study were obtained from Sigma-Aldrich. In this study, all of the chemicals were utilized without any additional purification.

2.2 Fabrication of Nano-SiO₂

The nano-SiO₂ was synthesized via the sol-gel technique (Dubey et al., 2015). 2.5 mL acetic acid was added to 5 mL tetraethyl orthosilicate (TEOS) solution under continuous mixing for 10 min. Then, 5 mL of 10 wt % solution of PVP in ethanol was poured dropwise into the above-mentioned mixture and the solution was stirred for 1 h to make a sol. To evaporate the water and organic components, the produced gel was dried at 90 °C for 3 h. Finally, the resulting gel was calcined at 600 °C for 3 h and then ground well into a fine powder via a porcelain mortar.

2.3 Characterization of the Synthesized Nano-SiO₂

X-ray spectra of the prepared nano-SiO₂ were specified using Shimadzu XRD-6100 with Cu-K_α radiation ($\lambda = 1.54 \text{ \AA}$) at 30 kV and 30 mA to examine the crystallinity of the synthesized material. The prepared nanopowder material was placed into a flat aluminum holder. The scan velocity was set at 2° min⁻¹ from 5 to 80°. The functional groups of the fabricated nano-SiO₂ were investigated via Fourier transform infrared spectroscopy (Shimadzu, FTIR-8400S), over a wavelength range of 4000–400 cm⁻¹. The morphological structure and chemical composition of the synthesized nano-SiO₂ were detected by transmission electron microscopy (TEM) coupled with energy-dispersive X-ray spectroscopy (EDS) (JEOL JSM-6010LV). Furthermore, the thermal stability of the prepared nano-SiO₂ was characterized using a thermogravimetric analyzer (TGA, SII 6300, Exstar). Briefly, specific amounts of nano-SiO₂ were placed into TGA pans and heated up to 1000 °C under N₂ gas flow with a heating rate of 10 °C/min, and the weight loss of the material was recorded. Moreover, the Brunauer-Emmett-Teller (BET) surface area analysis (Beckman Coulter SA3100, Brea, CA, USA) was used for the measurement of the surface area and the pore size of the fabricated nano-SiO₂, through the measurement of N₂ adsorption-desorption isotherms at 77 K. Before measurements, all samples were degassed under vacuum for 12 h at 25 °C. The zeta potential of nano-SiO₂ was measured by the zetasizer Nano series (Malvern Nano-Zs, model ZEN3600, UK). Before measurement, 0.01 g of the prepared sample was added to 10 mL of distilled water and sonicated for 20 min using the Flac-Ultrasonic (Baths 2020, model

LBS2 10 LT). At room temperature (25–30 °C), the zeta potential of nano-SiO₂ was determined at refractive index of 1.7, adsorption 0.01, viscosity 0.8872, and refractive index of solvent (water) of 1.33, with a dielectric constant of 78.5. The sample was measured in triplicate.

2.4 Experimental Design and Procedures

Both metals (i.e., Pb (II) and Cr (VI)) were examined individually and simultaneously. Therefore, two parallel sets of batch experiments were conducted to evaluate the adsorption performance of synthesized nano-SiO₂ toward the removal of lead and chromium. Each series consisted of five sequential experiments (a total of ten experiments), to investigate the influence of several operational parameters on the adsorption efficiency including contact time (0–180 min), initial pH (1–11), nano-SiO₂ dose (0.1–8 g L⁻¹), initial heavy metal concentration (5–100 mg L⁻¹), and temperature (room temperature–85 °C), respectively. These values have been selected according to the different standard values used in most of the former (Salama et al., 2022a, b, c; Shokry et al., 2020). In the beginning, single-metal stock solutions (individual metal) of Pb (II) and Cr (VI) with the chosen concentrations were prepared by dissolving lead nitrate; Pb(NO₃)₂, and potassium dichromate (K₂Cr₂O₇) in distilled water; then, stock solutions were kept in volumetric flasks in the dark at 4 °C, and the experimental work was designed as follows.

The first experiment was designed to assess the effect of contact time, where a certain dose of 1 g L⁻¹ of synthesized nano-SiO₂ was mixed with the artificial heavy metal-contaminated solutions in a 1-L glass beaker of a constant concentration of 10 mg L⁻¹ of each heavy metal, at a constant pH value of 7, and room temperature, for 180 min. At specific intervals, which ranged from 5 to 180 min, samples of the suspension solutions were extracted with a 5-mL syringe and then filtered and analyzed to determine the optimal contact time for each metal.

Secondly, to examine the influence of the initial pH value, using the optimal contact time of each heavy metal, where the same operating conditions of the previous adsorption experiment were kept constant except for the initial pH value, the pH values of the metallic solutions were modified using 0.1 M of NaOH or HCl and the pH range of 1–11 was

investigated. After that, the metal ion concentrations and removal efficiencies were assessed. According to the resulting removal observations, the optimum pH values were highlighted. Thirdly, the range of adsorbent dose of 0.1–8 g L⁻¹ was investigated, at the optimum operational conditions and ambient temperature.

Next, the impact of initial heavy metal ion concentration (5–100 mg L⁻¹) on the removal efficiency was examined at the resulting optimal contact time, initial pH value, nano-SiO₂ dose, and ambient temperature. Lastly, to explore the effect of reaction temperature on the removal efficiency, using the optimal contact time, dose, initial pH value, and ion concentration, the temperature range of (average room temperature 30–85 °C) was tested.

A typical lab-scale jar tester was used for all of the experiments. It mainly involves six graded cylinders with a 1-L capacity, six impellers placed on stainless steel shafts, and a variable-speed motor. Two 90° turbine blades with a 5 cm diameter and 2 cm height make up the impeller. There was a 0 to 200 rpm range for the impeller rotation speed. The optimum rotational speed was kept constant throughout all experiments at 150 rpm.

The desired initial pH value was adjusted with 0.1 M of NaOH or HCl (when needed); however, the medium pH was not controlled during the experiment. The validity of the resulting data was proved by doing all adsorption experiments in triplicate. Additionally, at the end of each experiment, duplicate samples of the suspension solutions were extracted, filtered, and analyzed, and the mean values were applied in data analysis. Following the completion of the water treatment experiments, the final pollutant concentration was determined and the pollutant removal percentage by synthesized nano-SiO₂ was calculated using Eq. (1):

$$\text{Removal\%} = \left[\frac{C_o - C_e}{C_o} \right] * 100 \quad (1)$$

where C_o is the initial pollutant concentration (mg L⁻¹), and C_e is the final concentration (mg L⁻¹). The adsorption capacity (mg g⁻¹) was calculated using the following equation:

$$q_e = \frac{V(C_o - C_e)}{m} \quad (2)$$

where V denotes the solution volume (L), and m denotes the mass of the fabricated nano-SiO₂ (g).

2.5 Equilibrium, Kinetics, and Thermodynamic Adsorption Behavior of Nano-SiO₂

Thermodynamic parameters of the adsorption process towards the investigated water contaminants (i.e., Pb (II) and Cr (VI)) were assessed in order to examine the nature of adsorption processes onto the fabricated nano-SiO₂. Furthermore, using the Langmuir, Freundlich, and Temkin isothermal equations, the equilibrium behavior of the adsorption processes onto nano-SiO₂ was evaluated. Pseudo-first-order, pseudo-second-order, Elovich, and intraparticle kinetic models were used to assess adsorption kinetics.

2.5.1 Thermodynamic Modeling for the Adsorption Process

The variations in enthalpy (ΔH°), standard free energy (ΔG°), and entropy (ΔS°) are the main thermodynamic characteristics that should be considered to explore the nature of any adsorption process. Using the Van't Hoff equation, the values of the standard enthalpy and entropy may be determined as follows (Walker, 1913):

$$\ln K_c = \frac{\Delta S^\circ}{R} - \frac{\Delta H^\circ}{RT} \quad (3)$$

where T is the solution's temperature in Kelvin; R is the universal gas constant, equal to 8.314 J mol⁻¹ K⁻¹; K_c is given by $F_e/(1 - F_e)$; and $F_e = (C_e - C_0)/C_0$ is the portion adsorbed at equilibrium. The intercept and the slope of the Van't Hoff plot are used to drive the values of ΔS° and ΔH° , respectively. Moreover, the following equation allows for the determination of the activation energy (E_a) (Lord & Kittelberger, 1974):

$$E_a = \Delta H^\circ + RT \quad (4)$$

2.5.2 Equilibrium Isotherm Analysis for Adsorption of Pb (II) and Cr (VI)

To study the adsorption behavior of the synthesized nano-SiO₂ for Pb (II) and Cr (VI) decontamination, the Langmuir, Freundlich, and Temkin models were

used. The C_e/q_e versus C_e plot of the Langmuir linearized can be made as follows:

$$\frac{C_e}{q_e} = \frac{1}{q_{\max} \cdot K_L} + \frac{C_e}{q_{\max}} \quad (5)$$

where C_e is the equilibrium concentration of the adsorbate (mg L⁻¹), q_e is the quantity of Pb (II) and Cr (VI) adsorbed at equilibrium (mg g⁻¹), K_L and q_{\max} are the Langmuir constants referred to as the adsorption energy (L mg⁻¹) and maximum monolayer adsorption capacity (mg g⁻¹), respectively (Langmuir, 1916).

Additionally, $\log q_e$ was plotted against $\log C_e$ to study the equilibrium data using Freundlich linear (Eq. (5)), where n_F and K_F are Freundlich constants correlated to the intensity and capacity of adsorption, respectively (Freundlich, 1906). The Temkin isotherm model, which is expressed as in Eq. (6), was used to examine the adsorption data of Pb (II) and Cr (VI) onto the synthesized nano-SiO₂, where A is the Temkin isotherm constant (L g⁻¹), and $B = RT/b$ is constant correlated to adsorption heat (J mol⁻¹) (Temkin, 1940):

$$\log q_e = \log K_F + \frac{1}{n_F} \log C_e \quad (6)$$

$$q_e = B \ln A + B \ln C_e \quad (7)$$

2.5.3 Kinetic Models of Pb (II) and Cr (VI) Adsorption

The pseudo-first order, pseudo-second order, Elovich, and intraparticle diffusion kinetic models were used to analyze the mechanism and kinetics for the adsorption process of Pb (II) and Cr (VI) onto the fabricated nano-SiO₂ from aqueous solution. As shown, the Lagergren first-order equation may be written as follows (Lagergren, 1898):

$$\ln(q_e - q_t) = \ln q_e - k_1 t \quad (8)$$

where the quantities of adsorbed Pb (II) and Cr (VI) ions (mg g⁻¹) at time t (min) and equilibrium are denoted by q_e and q_t , respectively, and the rate constant for the first-order reaction is k_1 (min). Moreover, the pseudo-second-order kinetic model was used

to examine the decontamination kinetic data and is depicted as follows (Blanchard et al., 1984):

$$t/q_t = (1/k_2 q_e^2) + t/q_e \quad (9)$$

where k_2 ($\text{g mg}^{-1} \text{min}^{-1}$) is the second-order rate's constant. Additionally, the Elovich equation was studied for the adsorption of many water contaminants by Weber and Morris (1963):

$$q_t = \beta \ln(\alpha \beta t) \quad (10)$$

where α is the initial adsorption rate ($\text{mg g}^{-1} \text{min}^{-1}$) and β is related to the activation energy of adsorption (g mg^{-1}) and the level of surface coverage. The slope and intercept of the linear plot of q_t against $\ln t$ can be used to derive the values of α and β , respectively. Finally, Weber and Morris's equation was used to investigate the potential effect of intraparticle diffusion on the adsorption process for the studied contaminants:

$$q_t = k_i t^{1/2} + C \quad (11)$$

where k_i is the intraparticle diffusion rate constant, and C values provide an estimation of the boundary layer's thickness. If intraparticle diffusion does take place, q_t against $t^{1/2}$ will be linear, and the rate-limiting mechanism will only be due to intraparticle diffusion if the plot passes through the origin. If not, a different mechanism in addition to intraparticle diffusion is at work (Largitte & Pasquier, 2016).

2.6 Instruments and Analytical Methods

A series of flocculators with six independent positions (Jar Tester, VELP Scientifica company, Model FC6S, USA) was used to conduct the experiments. The pH value and temperature were measured by a pH-ORP-TEMP Bench Meter (Adwa, Model AD1030, Hungary). An atomic absorption spectrophotometer (HACH, Model DR6000) was used for the analysis of heavy metals present in the solution. The AAS was conducted at wavelengths, λ_{max} (nm) of 217 and 357.9, height of 7 and 8 mm, specific current of 75 and 100%, and fuel flow of 1.2 and 1.3 L/min for Pb and Cr, respectively.

2.7 Regeneration of Synthesized Nano-SiO₂

For desorption and reusability studies, 1 g of the used nano-SiO₂ was recovered and washed three times with distilled water and 50 mL of methanol at 23 °C, agitated at 150 rpm for 10 min to elute the two tested model contaminants, and dried at 150 °C overnight for use in the subsequent adsorption experiments. Then, the re-adsorption processes were performed at the following optimized removal conditions: contact time = 60 and 90 min, pH = 5 and 2, nano-SiO₂ dosage = 0.5 and 1 g L⁻¹, and initial metal concentration = 10 ppm, for Pb (II) and Cr (VI), respectively, at room temperature.

3 Results and Discussion

3.1 Physicochemical Characteristics of the Fabricated Nano-SiO₂

XRD pattern of the prepared nano-SiO₂ is provided in Fig. 1. A typical broadband centered at $2\theta = 23.08^\circ$ is detected, which can be allocated to the nano-SiO₂ (Al Tbeishat, 2022). Moreover, no other diffraction peaks can be noted. Figure 1 confirms that the X-ray diffractogram illustrated the amorphous nature of the prepared nano-SiO₂ (Sharma et al., 2022).

Figure 2 shows the FTIR spectrum of the fabricated nano-SiO₂. The band at 798 cm^{-1} is attributed to the bending vibration of Si-O (Diab et al., 2021)

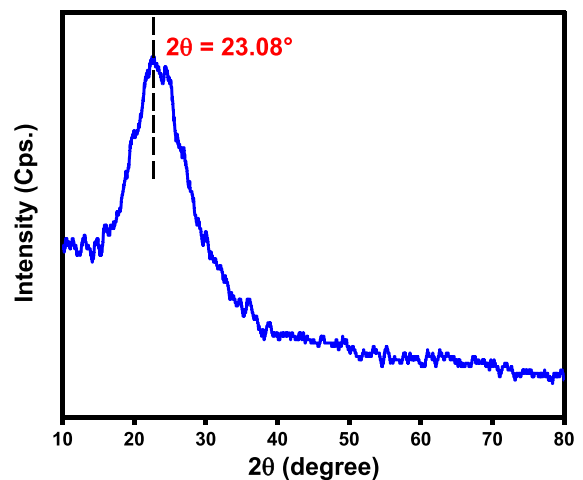


Fig. 1 XRD patterns of the synthesized nano-SiO₂

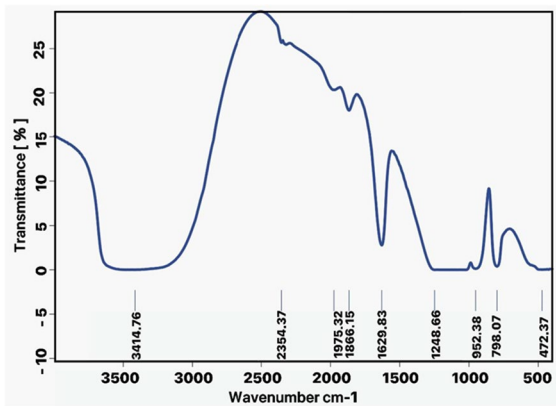


Fig. 2 FTIR spectra of the fabricated nano-SiO₂

where the oxygen moves at the right angle to the Si–Si lines in the Si–O–Si plane (Afanador-Delgado et al., 2022). The absorption observed at 952 cm⁻¹ matches the stretching vibration of Si–OH. The above-mentioned FTIR results demonstrated outstanding nano-SiO₂ fabrication (Dubey et al., 2015).

In Fig. 3, the TEM and EDX images of the synthesized nano-SiO₂ are shown. The TEM images reaffirmed a chain-like agglomeration of nanoparticles. The particle size swung from 50 to 75 nm, and the NPs had a semi-spherical shape with a low tendency to aggregate. On the contrary, the elemental mapping (Fig. 3B–D) illustrated the presence of Si and O in the synthesized nanomaterial. Additionally, the EDX pattern of nano-SiO₂ in Fig. 3E demonstrated the existence of the elements.

Thermogravimetric analysis (TGA) of the prepared nano-SiO₂ is shown in Fig. 4, where two main degradation stages were detected. The first degradation step of 13.16% at 113 °C may be due to the loss of water molecules and atmospheric gases that are combined with the fabricated nano-SiO₂ (Samy et al., 2023). The second degradation stage with a total weight loss of 10.36% swung from 113 to 988 °C which was assigned to the cleavage of the backbone of the synthesized nano-SiO₂ (Salama et al., 2015). According to these data, the prepared nano-SiO₂ elucidated excellent thermal characteristics compared with other nanomaterials (Elkady et al., 2020; Saad et al., 2022).

Figure 5 shows the fabricated nano-SiO₂'s adsorption-desorption curve. Both the total pore diameter and the specific surface area of the produced nano-SiO₂ were determined to be 0.104 cm³ g⁻¹ and 78.38

m² g⁻¹, respectively. From the above-mentioned outcomes, the synthesized nano-SiO₂ achieved a significantly high surface area, which confirms its potential applicability to adsorb the pollutants from wastewater (Kumar et al., 2022).

3.2 Application of Synthesized Nano-SiO₂ for Pb (II) and Cr (VI) Adsorption

Using the batch method at room temperature, the feasibility of Pb (II) and Cr (VI) adsorption onto the fabricated nano-SiO₂ from aqueous solutions was examined. In addition, the impact of contact time, initial pH value, nano-SiO₂ dose, initial pollutant concentration, and temperature was investigated according to the experimental design that was previously reported (Salama et al., 2022a, b, c; Shokry et al., 2020), to set the optimal operating parameters controlling the adsorption process.

3.2.1 Effect of Contact Time

The influence of contact time on the removal efficiency of Pb (II) and Cr (VI) using 1 g L⁻¹ from the prepared nano-SiO₂ was investigated over 180 min, and the change in the concentration of the metals at specific time intervals was monitored, as presented in Fig. 6. The obtained results indicated that the metal ion removal rate was rapid at the initial period until the equilibrium state was reached. Then, the adsorption rate slowed down, and a slight increase was recorded irrespective of time. The large accessible surface area and functional groups of the fabricated nano-SiO₂ material may be responsible for this high adsorption rate in the first phase, which causes a faster collision velocity between the metal ions and the adsorption sites (Diab et al., 2021). On the other hand, in the second phase of adsorption, after equilibrium, the active sites were saturated with metal ions, and the adsorbent surface became exhausted, limiting further uptake and constituting a non-significant adsorption rate (Mehdinia et al., 2021). According to these results, at neutral pH, the optimum equilibrium time for the adsorption of Pb and Cr onto the prepared nano-SiO₂ was considered 60 and 90 min, with the highest removal percentage of 84.46 and 65.5%, respectively; additional time could not cause any significant removal. Similar trends were previously registered in the literature (i.e., 60 and 90 min for Pb and

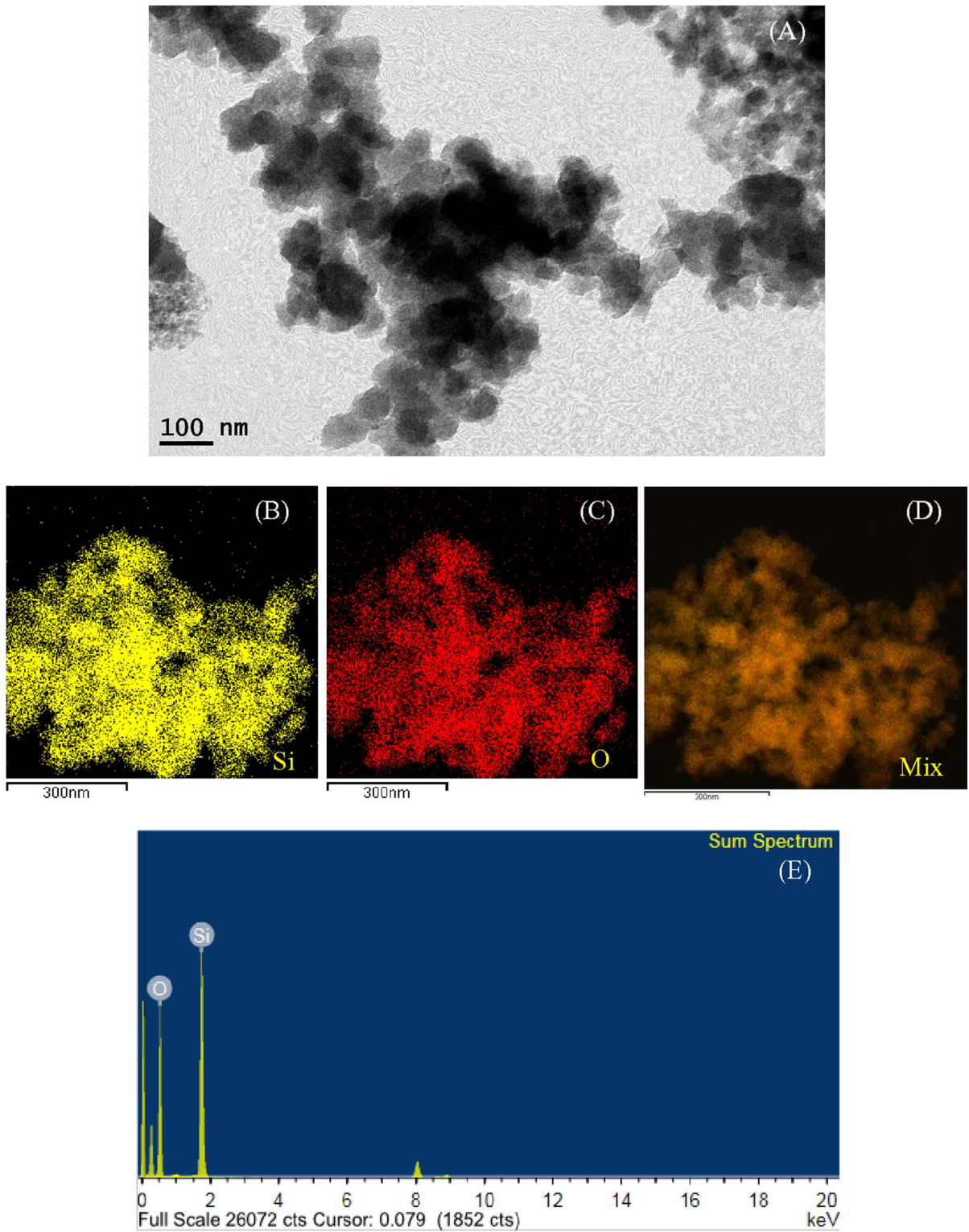


Fig. 3 TEM, elemental mapping, and EDX images of the fabricated nano-SiO₂

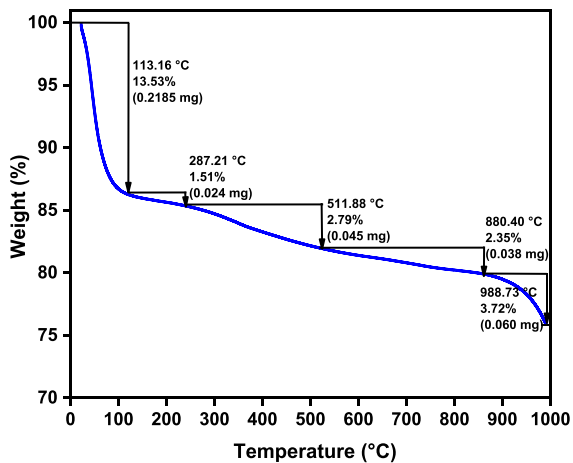


Fig. 4 TGA curve of the synthesized nano-SiO₂

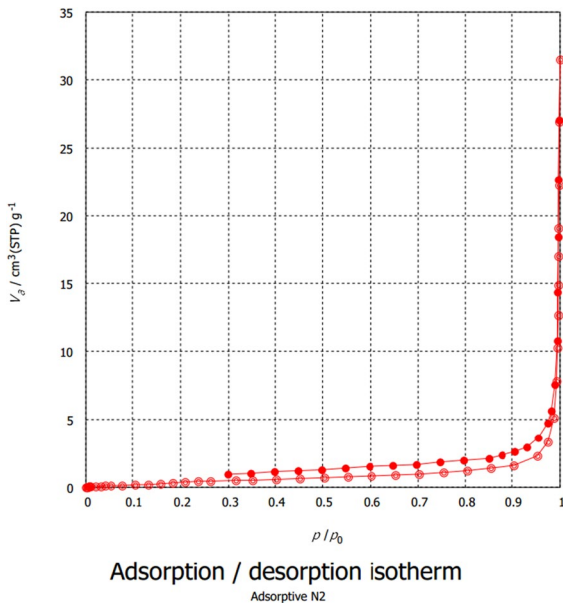


Fig. 5 Adsorption/desorption isotherm of the prepared nano-SiO₂

Cr, respectively (Godini et al., 2020; Tan et al., 2012; Xiao et al., 2017; Xiong et al., 2019).

Moreover, the prepared nano-SiO₂ represents an efficient and time-saving adsorbent for heavy metals compared with other previously prepared nanoparticles such as carbon nanotubes (CNTs) (Rahbari & Goharrizi, 2009), copper ferrite nanoparticles (CuFe₂O₄) (Tu et al., 2017), and CuO nanoparticles

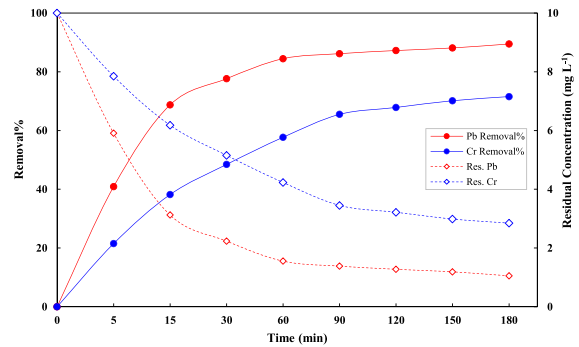


Fig. 6 Effect of contact time on the removal efficiency of Pb (II) and Cr (VI) using nano-SiO₂ (operational conditions: initial pH=7, nano-adsorbent dose=1 g L⁻¹, initial metal concentration=10 mg L⁻¹, at room temperature)

(Verma et al., 2017a) that recorded 360, 220, and 100 min optimal contact time, respectively, for the removal of 10 mg L⁻¹ initial Pb concentration, and compared with Cr removal within 240 and 180 min, using alumina nanoparticles immobilized zeolite (Al₂O₃ NPs in zeolite) (Deravanesiyan et al., 2015) and tetraethylenepentamine-functionalized nano-magnetic polymer (TEPA-NMPs) (Shen et al., 2013), respectively.

Additionally, higher removal rates of Pb (II) were observed along the experiment period, as compared to those in Cr (VI) under the same operational conditions as shown in Fig. 6, as suggested by the hard acid soft base (HSAB) hypothesis, which describes metal ion interactions based on their underlying chemistry; both the type of the metals and their species in the solution have a role in adsorbent-metal binding. According to the HSAB theory, the hardness of the two metals examined in this study can be classified as Cr (VI) > Pb (II) (Pearson, 1968; Soon et al., 2022). Overall, these results demonstrated the crucial effect of contact time on the Pb (II) and Cr (VI) adsorption process onto the fabricated nano-SiO₂.

3.2.2 Effect of pH

In the adsorption process, solution pH is crucial; it influences both the contaminants' ionization level and the adsorbent's surface charge (Kuang et al., 2020). Therefore, the effect of pH on the adsorption process was investigated at a range from 1 to 11, and it was noted that the initial pH values of 5 and 2 were favorable for the Pb (II) and Cr (VI) adsorption onto

fabricated nano-SiO₂ (under the same conditions), respectively. The results indicated that increasing the initial pH from 1 to 5 significantly increased Pb (II) removal efficiency (Fig. 7a); then, an inconsiderable removal efficiency was recorded with the progressed increase in pH from 5 to 11. Subsequently, the initial pH value of 5 was picked as the optimum pH for the adsorption of Pb (II) onto synthesized nano-SiO₂. This is consistent with the optimum pH for the adsorption of Pb (II) using nanoparticles reported by similar studies (Tan et al., 2012; Yuan et al., 2018; Zhu et al., 2017), which tested different pH values and found that the optimum pH value was 5.

Conversely, the results demonstrated that for Cr (VI), the removal efficiency was inversely proportional to the initial pH values, and the removal efficiency was shown to drop, going from 82 to 31.5% as the initial pH value raised from 1 to 11 as shown in Fig. 7a. The initial pH value of 2 was picked as the optimum pH for the adsorption of Cr (VI) onto

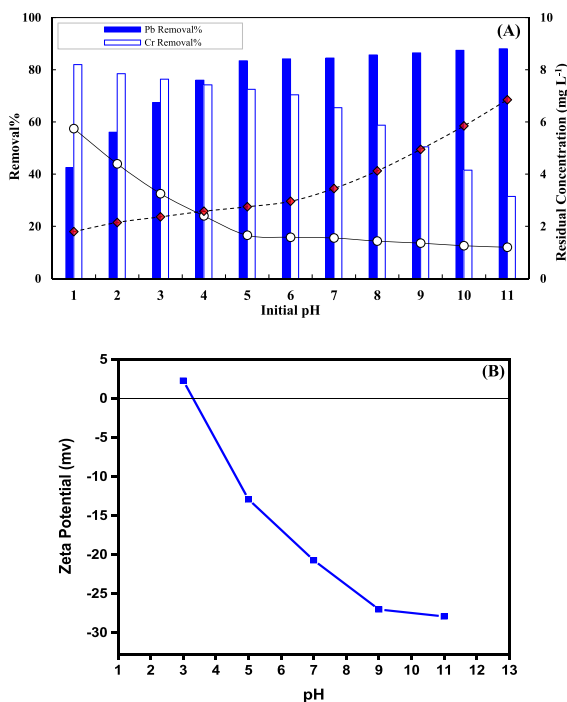


Fig. 7 A Effect of pH on the removal efficiency of Pb (II) and Cr (VI) using nano-SiO₂ (operational conditions: nano-adsorbent dose = 1 g L⁻¹, initial metal concentration = 10 mg L⁻¹, and contact time = 60 and 90 min for Pb and Cr; respectively, at room temperature). B Zeta potential of nano-SiO₂ as a function of pH value

synthesized nano-SiO₂, although the highest removal efficiency was achieved at a pH of 1. This was done to mitigate the negative impacts of extremely strong acidic circumstances, which are known to damage materials, corrode surfaces, and alter the chemical composition of the substances involved in the adsorption process. This could hinder the intended interactions between the adsorbent and adsorbate, decreasing the efficiency of the adsorption process. Additionally, strong acids might denature or degrade the adsorbent material, rendering it ineffective or causing it to lose its adsorption capacity. Besides, due to the marginal disparity between the two removal values (82% at pH 1 and 78.5% at pH 2), we opted for pH 2 to be the optimal value. This result is totally consistent with the previously published research (Jain et al., 2018; Samrot et al., 2019; Xu et al., 2015).

The explanation for the adsorption mechanism of Pb (II) and Cr (VI) onto nano-SiO₂ at different pHs can be due to both the point of zero charge (pzc) for SiO₂ and relative distribution of Pb and Cr species as a function of pH in the solution. The pzc for SiO₂ was reported to be around 3 (Goynes et al., 2002). Furthermore, when pH falls below 3, the synthesized nano-SiO₂'s zeta potential data (Fig. 7b) shows that it has reached the isoelectrical point, which is the point at which the positive and negative charges produced by the silanol groups on the surface of the silica particles are equal. The silanol groups with the Si-OH structure are stable at that moment. The zeta potential grows in negative proportion as the pH value rises over 3.5, signifying a rise in the amount of negative charges on the particle surface. The equilibrium of the SiOH/SiO⁻ acid/base dissociation means that an increase in negative charges will lead to an increase in SiO⁻ species and the surface energy (Xu et al., 2006). Subsequently, the surface of SiO₂ is positively charged at any pH value below the pzc and negatively charged at any pH value over the pzc. For Pb (II), the surface of the synthesized nano-SiO₂ is positively charged at low pH values (pH < 3), so there is a repulsion force between the positively charged Pb (II) and the positively charged surface of synthesized nano-SiO₂. Otherwise, when the pH of the solution increases (pH > 3), the surface of the synthesized nano-SiO₂ becomes negatively charged, and as a result, the adsorption of positively charged Pb (II) is enhanced due to the electrostatic attraction. While Cr (VI) species are present in negative forms in the

aqueous solution, therefore, the maximum adsorption was distinguished in the acid circumstances ($\text{pH} < 3$).

3.2.3 Effect of Nano-SiO₂ Dosage on the Adsorption Process

The adsorbent dosage is one of the adsorption process' most important parameters since it has a strong effect on the adsorbent capacity at a constant initial pollutant concentration (Gouamid et al., 2013). For this reason, the effect of the synthesized nano-SiO₂ dosage on both Pb (II) and Cr (VI) removal was investigated, utilizing the range of (0.1–8 g L⁻¹), as shown in Fig. 8. As seen in the figure, it can be realized that the removal efficiency was considerably enhanced by increasing nano-SiO₂ dosage from 0.1 to 0.5 g L⁻¹ for Pb (II) and from 0.1 to 1 g L⁻¹ for Cr (VI), respectively. After that point, a minor increase in removal percentages was noted with the continued increase to 8 g L⁻¹. The resultant trend was informed by various related studies (Ali et al., 2021; Elkady et al., 2017, 2016a, b; Rahmani et al., 2011; Shahbazi et al., 2012). These findings may serve as evidence that when nano-SiO₂ concentrations increase, more active sites become available for the adsorption of heavy metal ions (Salama et al., 2022a, b, c; Thinakaran et al., 2008). On the other hand, the degradation in the ability of nano-SiO₂ to adsorb the tested pollutants at high dosages may be due to the unsaturated adsorption residual sites on its surface (Rahmani et al., 2011; Shahbazi et al., 2012). Consequently, based on the observed results, the optimum

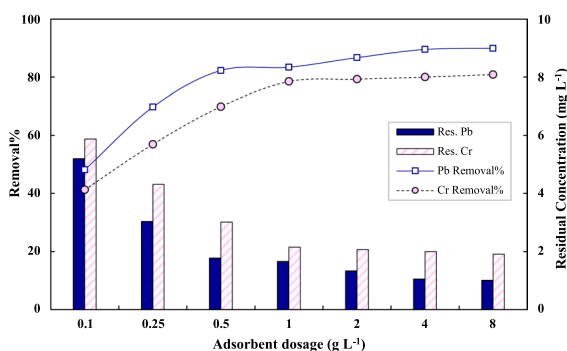


Fig. 8 Effect of nano-SiO₂ dose on the adsorption of Pb (II) and Cr (VI) (Operational conditions: contact time = 60 and 90 min, pH = 5 and 2, and initial metal concentration = 10 mg L⁻¹, for Pb (II) and Cr (VI), respectively), at room temperature

dosages of the synthesized nano-SiO₂ were picked as 0.5 and 1 g L⁻¹ for Pb (II) and Cr (VI), respectively, which are suggested as economically reasonable dosages for the adsorption processes. These values were confirmed by the optimum dose for the adsorption of Pb (II) and Cr (VI) reported by Rahbari and Goharizi (Rahbari & Goharizi, 2009) and Hosseini et al. (Hosseini et al., 2019), who examined several dosages and found that the optimum was 0.5 and 1 g L⁻¹ for Pb (II) and Cr (VI), respectively.

3.2.4 Effect of Initial Pb (II) and Cr (VI) Concentration on the Removal Performance

Using the optimal contact time, initial solution pH, and nano-SiO₂ dose, for each metal, separately, the impact of the initial concentration of Pb (II) and Cr (VI) was examined within the range of 5 to 100 mg L⁻¹. Figure 9 demonstrates that for both metals, the removal efficiency was inversely proportional to the initial concentration. The obtained results indicated that removal efficiency was shown to drop, going from 87.2 to 49.16% and from 81.5 to 43.3% as the initial concentration raised from 5 to 100 mg L⁻¹ for Pb (II) and Cr (VI), respectively. On the contrary, the adsorption capacities were improved as the initial concentration rose from 5 to 100 mg L⁻¹. The obtained results are totally consistent with the previously published research (Diab et al., 2021; Elkady et al., 2017, 2016a, b; Hassan et al., 2017). This trend may be related to the inability of the fabricated nano-SiO₂ to provide the active sites required for the higher

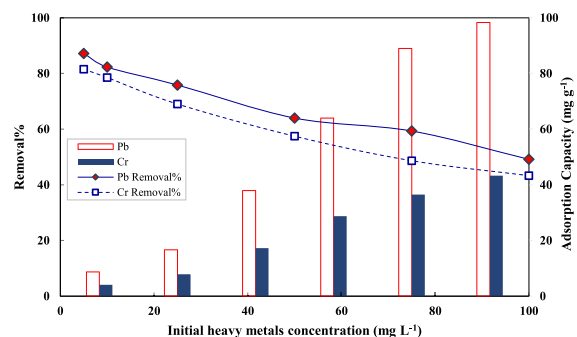


Fig. 9 Effect of initial concentrations of Pb (II) and Cr (VI) ions on the adsorption efficiency and capacity of the fabricated nano-SiO₂ at the optimal conditions (i.e., contact time = 60 and 90 min, pH = 5 and 2, nano-SiO₂ dosage = 0.5 and 1 g L⁻¹, for Pb (II) and Cr (VI), respectively), at room temperature

concentrations of Pb (II) and Cr (VI). The active sites on the nano-SiO₂ are sufficient for Pb (II) and Cr (VI) reduction and adsorption in the case of low quantities of these metals. High metal ion concentrations, on the other hand, prevent the proper interaction between the adsorbents and metal ions because the reactive sites are unable to absorb (Wen et al., 2022). Our findings demonstrated the effectiveness of the synthesized nano-SiO₂ in the Pb (II) and Cr (VI) decontamination of aqueous solutions at different initial concentrations.

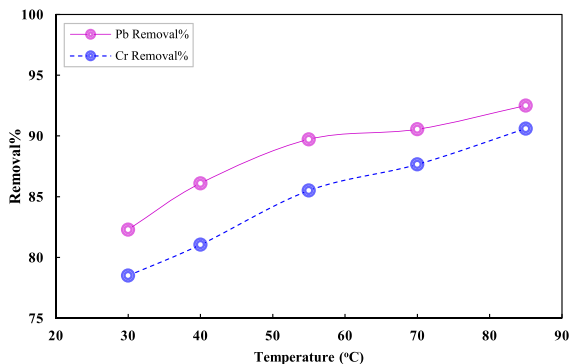
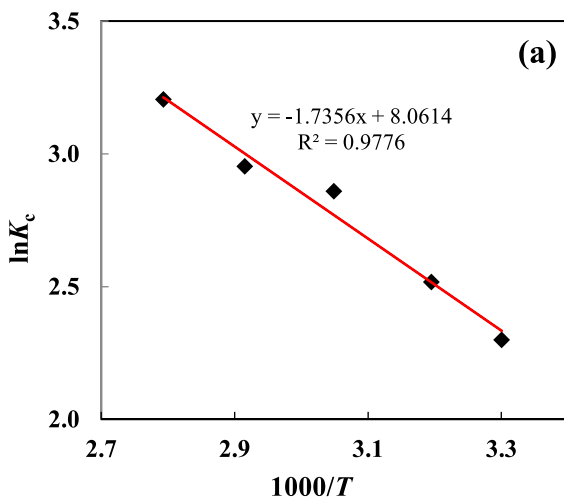


Fig. 10 Effect of solution temperature on the percentage of Pb (II) and Cr (VI) removal efficiency onto the fabricated nano-SiO₂ at the optimal operational conditions (i.e., contact time=60 and 90 min, pH=5 and 2, nano-SiO₂ dosage=0.5 and 1 g L⁻¹, and initial metal concentration=10 mg L⁻¹, for Pb (II) and Cr (VI), respectively)



3.2.5 Effect of Solution Temperature on the Heavy Metals' Removal Efficiency

Figure 10 elucidates the impact of temperature on Pb (II) and Cr (VI) removal efficiency using the fabricated nano-SiO₂. The adsorption of both Pb (II) and Cr (VI) was shown to increase as the solution temperatures raised from 30 to 85°C, demonstrating that high temperatures were favorable for the adsorption process. This behavior may be due to the development of other adsorption sites onto the nano-SiO₂ at higher temperatures, which enhances the diffusion rate of the metal ions into the pores of the fabricated nano-SiO₂ (Elkady et al., 2016a, b). These results indicated that the Pb (II) and Cr (VI) adsorption onto the nano-SiO₂ is an endothermic process (Elkady et al., 2017; Salama et al., 2022a, b, c).

3.3 Equilibrium, Kinetics, and Thermodynamic Adsorption Behavior of Nano-SiO₂

3.3.1 Thermodynamic Modeling for the Adsorption Process

According to Fig. 11a and b, for various examined Pb (II) and Cr (VI) concentrations, the Van't Hoff plot of $\ln K_c$ versus $1000/T$ yields a straight line with a respectable value of correlation coefficient (R^2), and by using the intercept and slope of the Van't Hoff plot, the values of ΔS° and ΔH° were estimated. The

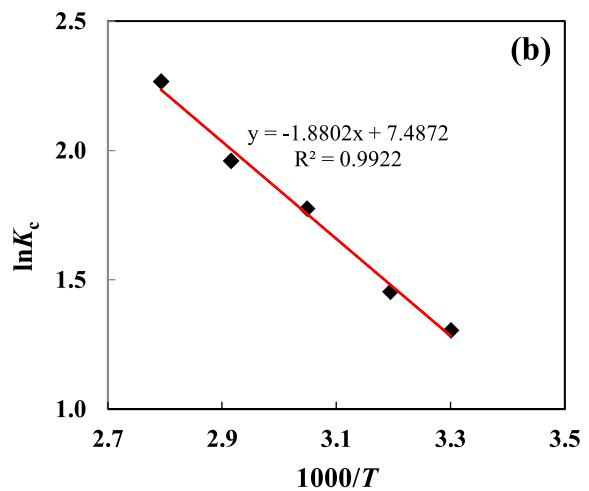


Fig. 11 The Van't Hoff plot of $\ln K_c$ against $1000/T$ for **a** Pb (II) and **b** Cr (VI) adsorption onto the fabricated nano-SiO₂

estimated thermodynamic parameters values of ΔH° , ΔG° , ΔS° , and E_a at various temperatures for Pb (II) and Cr (VI) are presented in Table 1. The spontaneous and thermodynamic nature of the adsorption process of Pb (II) and Cr (VI) onto the fabricated nano-SiO₂ is indicated by the negative values of free energy changes (ΔG°) (Elkady et al., 2017). On the other hand, the positive values of enthalpy (ΔH°) demonstrate that the adsorption processes are endothermic (Thinakaran et al., 2008). Yet, the increased disorder at the liquid/solid interface during the adsorption processes is illustrated by the positive values of entropy (ΔS°) (Diab et al., 2021).

3.3.2 Equilibrium Isotherm Analysis for Adsorption of Pb (II) and Cr (VI)

To study the adsorption behavior of the synthesized nano-SiO₂ for Pb (II) and Cr (VI) decontamination, the Langmuir, Freundlich, and Temkin models were used. The Langmuir linearized plot of C_e/q_e against C_e (Eq. (4)) gives a straight line with a high correlation coefficient ($R^2=0.984$ for Pb (II) and 0.99 for Cr (VI), respectively). The parameters of the examined equilibrium isotherm models are reported in Table 2,

and the constants for the isotherm models were calculated from the slope and intercept of the linear plots which are shown in Figs. 12 and 13. By comparing the three models' linearization fitting, it was revealed that Langmuir and Temkin's R^2 values were lower, indicating that the Freundlich model is the best match for describing the decontamination processes of Pb (II) and Cr (VI) onto nano-SiO₂. Besides, the Freundlich adsorption intensity (n_F) values were more than the unity and recorded 1.771 and 1.767 for the adsorption of Pb (II) and Cr (VI), respectively, showing that the adsorption processes onto the synthesized nano-SiO₂ are favorable (Üner et al., 2016). The Freundlich isotherm, which provides the best fit to the equilibrium data, predicts that metal ions would physically adsorb onto the synthesized nano-SiO₂ by multilayer adsorption on heterogeneous surfaces (Shokry Hassan, 2019).

3.3.3 Kinetic Models of Pb (II) and Cr (VI) Adsorption

The pseudo-first order, pseudo-second order, Elovich, and intraparticle diffusion kinetic models were used to analyze the mechanism and kinetics

Table 1 Thermodynamic parameters for Pb (II) and (VI) adsorption onto nano-SiO₂

Metal	Temp (K)	1000/T	K_c	$\ln K_c$	ΔG° (kJ·mol ⁻¹)	E_a (kJ·mol ⁻¹)	ΔH° (kJ·mol ⁻¹)	ΔS° (J·mol ⁻¹ ·K ⁻¹)
Pb (II)	303	3.30	9.97	2.30	-5.79	16.95	14.43	67.02
	313	3.19	12.39	2.52	-6.55	17.03		
	328	3.05	17.46	2.86	-7.80	17.16		
	343	2.92	19.16	2.95	-8.42	17.28		
	358	2.79	24.67	3.21	-9.54	17.41		
Cr (VI)	303	3.30	3.68	1.30	-3.29	18.15	15.63	62.25
	313	3.19	4.28	1.45	-3.78	18.23		
	328	3.05	5.90	1.77	-4.84	18.36		
	343	2.92	7.10	1.96	-5.59	18.48		
	358	2.79	9.64	2.27	-6.74	18.61		

Table 2 Isotherm parameters of Langmuir, Freundlich, and Temkin models for Pb (II) and Cr (VI) removal using the fabricated nano-SiO₂

Metal	Langmuir parameters			Freundlich parameters			Temkin parameters		
	q_m (mg g ⁻¹)	K_L (L mg ⁻¹)	R^2	K_F (mg g ⁻¹)	n_F	R^2	A (L g ⁻¹)	B (J mol ⁻¹)	R^2
Pb (II)	117.74	0.091	0.992	12.22	1.771	0.995	1.57	21.25	0.978
Cr (VI)	51.42	0.074	0.993	4.8	1.767	0.995	1.2	9.46	0.984

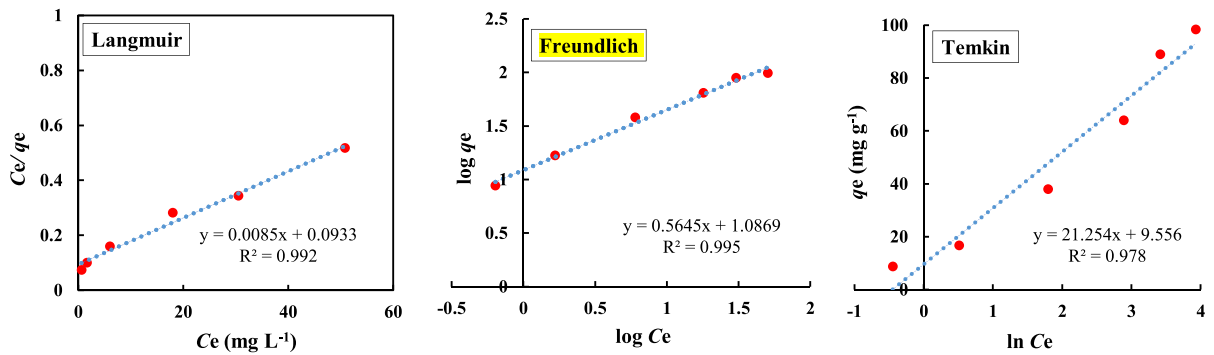


Fig. 12 Adsorption isotherms models: Langmuir, Freundlich, and Temkin, for Pb (II)

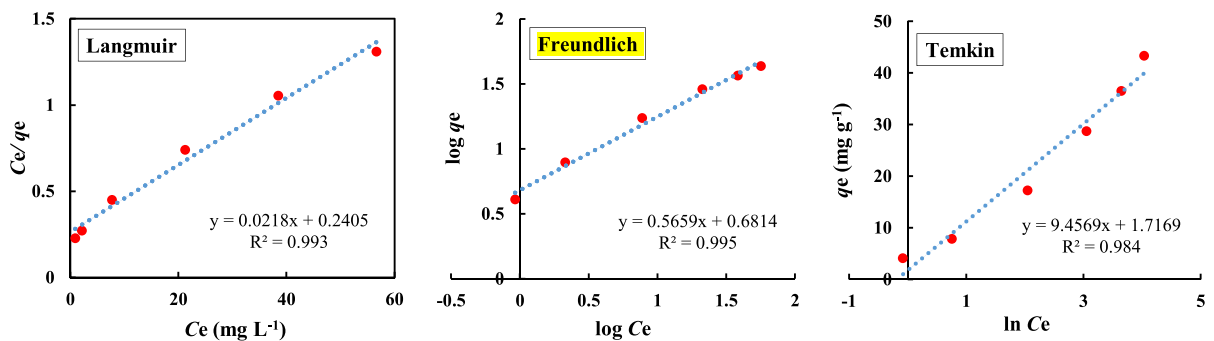


Fig. 13 Adsorption isotherms models: Langmuir, Freundlich, and Temkin, for Cr (VI)

for the adsorption process of Pb (II) and Cr (VI) onto the fabricated nano-SiO₂ from aqueous solution. The four examined kinetic models for the adsorption of Pb (II) and Cr (VI) ions onto the synthesized nano-SiO₂ from aqueous solutions were compared, and their correlation coefficient values for linear plotting are listed in Table 3. Yet, there was a considerable difference between experimental q_e and the attained q_e from the pseudo-first-order model, despite the high R^2 for pseudo-first-order. As a result, the pseudo-first-order model proved ineffective in explaining how Pb (II) and Cr (VI) were adsorbed on the nano-SiO₂ surface. Concerning the pseudo-second-order model, the model constants were estimated from the slope and the intercept of the linear relation between t/q_t and t . The significance of the pseudo-second-order model was confirmed by the high R^2 (0.999) and the lower difference between the experimental and estimated q_e from the model. These findings support the hypothesis that the Pb (II) and Cr (VI) adsorption

Table 3 Pseudo-first-order, pseudo-second-order, Elovich, and intraparticle diffusion kinetic parameters for Pb (II) and Cr (VI) removal onto nano-SiO₂

Kinetic model	Parameter	Value	
		Pb (II)	Cr (VI)
Pseudo-first order	$q_{exp.}$ (mg g ⁻¹)	8.42	7.87
	$q_{theor.}$ (mg g ⁻¹)	7.29	5.54
	K_1 (min ⁻¹)	0.07	
	R^2	0.997	0.996
Pseudo-second order	$q_{exp.}$ (mg g ⁻¹)	8.42	7.87
	$q_{theor.}$ (mg g ⁻¹)	9.1	8.9
	K_2 (g mg ⁻¹ min ⁻¹)	0.015	0.008
	R^2	0.999	0.999
Elovich kinetic model	α (mg g ⁻¹ min ⁻¹)	1.76	0.31
	β (g mg ⁻¹)	1.45	1.6
	R^2	0.957	0.994
Intraparticle diffusion kinetic model	C (mg g ⁻¹ min ⁻¹)	4.12	2.70
	k (g mg ⁻¹)	0.41	0.47
	R^2	0.75	0.902

processes were mostly governed by the pseudo-second kinetic model (Vikrant et al., 2017).

The Elovich model is a representative of understanding the kinetics of chemisorption. Table 3 lists the estimated Elovich parameters derived from the basic Elovich plot's slope and intercept, where β indicates the number of accessible sites for metal adsorption onto nano-SiO₂, while α indicates the amount of adsorption. The correlation coefficient value is rather low when compared to the pseudo-second-order, as presented in Table 3, suggesting that the Elovich model is adequate to describe the experimental results. This finding suggested that physical interaction may be the mechanism by which metals are adsorbed onto nano-SiO₂.

Lastly, the intraparticle diffusion model addressed the potential of intraparticle diffusion altering the adsorption process, which suggests if the adsorption process occurs via surface adsorption or intraparticle diffusion. Table 3 shows the values of k_i and C that were calculated from the slope and intercept. The value of C provides a forecast regarding the thickness of the boundary layer, where k_i represents the constant of the intraparticle diffusion rate. Metal ions were rapidly adsorbed on nano-SiO₂ during the first hour and subsequently diminished during the next 2 h. The main causes of the fast adsorption are either macropore diffusion or boundary layer diffusion. With a low R^2 value, the results predict that the adsorption process was uncontrolled by the intraparticle diffusion model.

3.4 Mechanism of the Removal of Heavy Metals

The following are the four main mechanisms that remove the metals: (1) *precipitation* which is the process by which mineral components or elements (such as SiO₄, Al, or Fe) precipitate in the solution or on the surface of the sorbent; (2) *electrostatic attraction* takes place between the adsorbent and metal ions, and it depends on the point of zero charge of the adsorbent, the pH of the solution, and the speciation of the metal; when $\text{pH} > \text{pH}_{\text{pzc}}$, the adsorbent's surface is negatively charged, which promotes the adsorption of metal cations; (3) *cation exchange*, a reversible chemical process that replaces metal cations on the surface of the sorbent with exchangeable metal ions (such as Ca²⁺, K⁺, Na⁺, and Al³⁺); (4) *surface complexation*, which is the result of a chemical interaction between

metal ions and oxygenated functional groups such as carboxyl, hydroxyl, or phenolic on the adsorbent's surface to generate metal complexes (Ambaye et al., 2020; Esfandiar et al., 2022).

The processes responsible for the removal of both investigated metals using fabricated nano-SiO₂ are mainly precipitation and electrostatic attraction as confirmed by the results of this study. First, the FTIR spectra before and after the adsorption processes were compared, as shown in Fig. 14. According to the obtained data, there was no chemical interaction or exchange between nano-SiO₂ and the metal ions, as evidenced by the non-significant changes in the FTIR spectrum of the nano-SiO₂ before and after the adsorption processes (negligible transitions in the peaks). Second, as discussed in the effect of initial

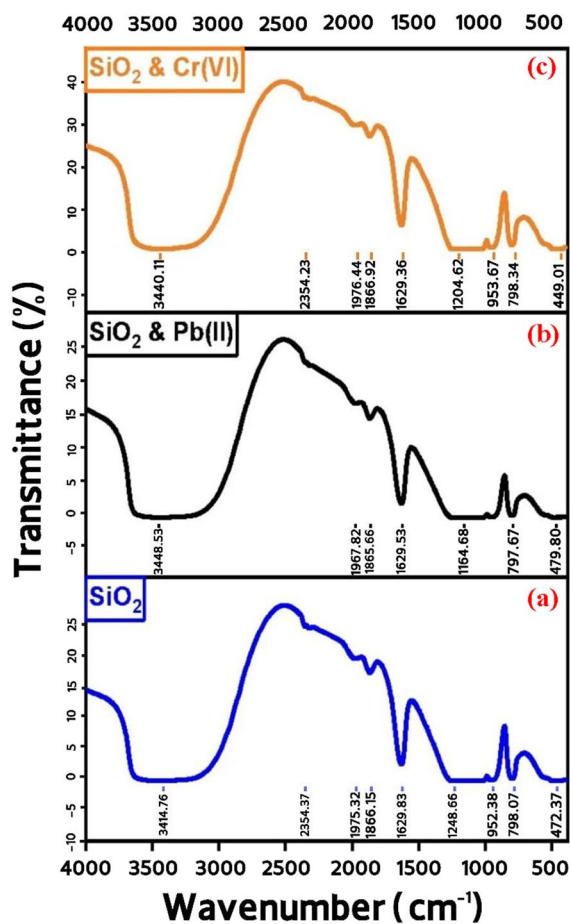


Fig. 14 Comparison of the FTIR spectra of **a** the synthesized nano-SiO₂, **b** nano-SiO₂ and Pb(II), and **c** nano-SiO₂ and Cr(VI)

pH on the adsorption process (Sect. 3.2.2), at solution $\text{pH} > 3$ (nano-SiO₂'s $\text{pH}_{\text{pzc}} = 3$), the nano-SiO₂'s surface is negatively charged and is expected to remove positively charged Pb (II) through electrostatic attraction, while at $\text{pH} < 3$, nano-SiO₂'s surface is positively charged and attracts the negative species of Cr (VI) presented in the aqueous solution. These results demonstrate that the mechanism of Pb (II) and Cr (VI) adsorption onto nano-SiO₂ could be categorized as the adsorbate and adsorbent material's physical interaction. This prediction was validated by the equilibrium analysis of the adsorption data, which showed that the adsorption process follows the Freundlich isotherm, and the predominant adsorption phenomenon is the multilayer adsorption mechanism, which confirms the physical interaction between the metal ions and the prepared nano-SiO₂. Finally, by comparing the R^2 values of the kinetics models (Sect. 3.3.3), it was indicated that the metal adsorption process can be described using the pseudo-second-order model. Therefore, the main adsorption mechanism proposed to take place is possibly physical adsorption.

3.5 Reusability of the Fabricated Nano-SiO₂

The excellent adsorbent should possess higher desorption ability without minor loss in adsorption capacity and selectivity over several adsorption cycles, as it affects the overall cost of practical applications (Bashir et al., 2021). Therefore, desorption and reusability experiments of the regenerated

nano-SiO₂ were conducted, where the recovered nano-SiO₂ was utilized six times for Pb (II) and Cr (VI) decontamination in order to evaluate its reusability affinity. As presented in Fig. 15, the results demonstrated excellent regeneration/reusability of nano-SiO₂ over six successive adsorption cycles, in which the removal efficiency decreased to 51.67% and 50% for Pb (II) and Cr (VI), respectively. According to the obtained results, the nano-SiO₂ proved good ability to be reused with an acceptable removal efficiency.

3.6 Performance Comparison of Nano-SiO₂ with Various Nano-adsorbents

The adsorption performance of the fabricated nano-SiO₂ with various previously investigated nano-adsorbents for decontamination of Pb (II) and Cr (VI) was compared based on maximum adsorption capacity (q_m), maximum removal efficiency, and optimum operating conditions as presented in Table 4 and 5. It was evident from the table that the synthesized nano-SiO₂ outperforms most of the reported nano-adsorbents. It was designated that the monolayer adsorption capacity of nano-SiO₂ is largest compared with other literature-studied materials. Moreover, the peak removal efficiency was higher as compared to other studies. More specifically, it possesses 3.1 and 1.8 times better removal efficiency for Pb (II) than wheat straw (Cao et al., 2019) and humic acid (Kushwaha et al., 2020), respectively. For Cr (VI) removal, it possesses 2.3

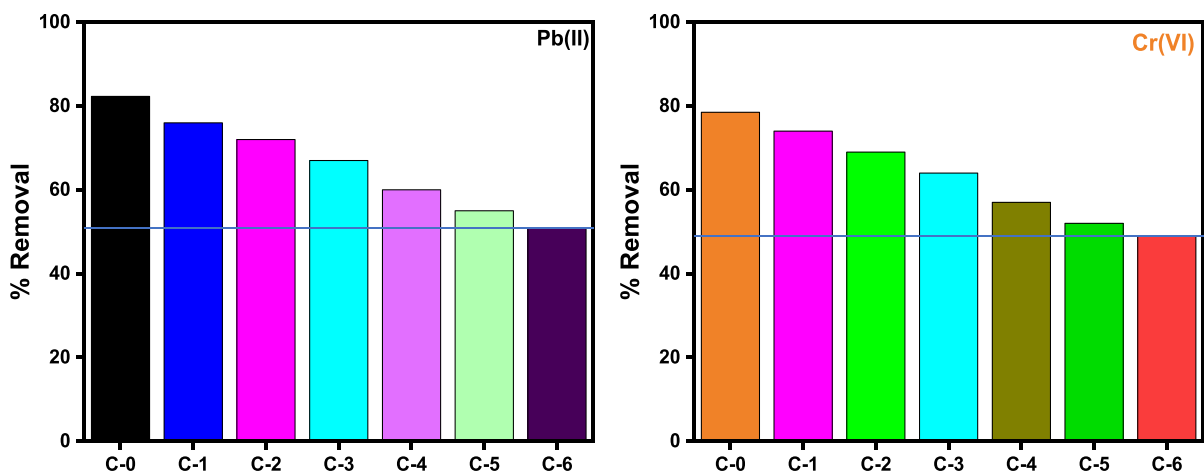


Fig. 15 Reusability of nano-SiO₂ for Pb (II) and Cr (VI) decontamination

Table 4 Performance comparison of Pb (II) adsorption on the synthesized nano-SiO₂ and various nano-adsorbents documented in the literature

Pollutant	Adsorbent	Optimum adsorption conditions	Maximum removal efficiency (%)	Maximum adsorption capacity (mg g ⁻¹)	Reference
Pb (II)	Nano-silica oxide	Time = 60 min Initial pH = 5 Dose = 0.5 g L ⁻¹ Conc. = 10 mg L ⁻¹	84.5	117.74	Present study
	Nano zero-valent iron (nZVI)	Time = 60 min Initial pH = 9 Dose = 0.1 g L ⁻¹ Conc. = 10 mg L ⁻¹	75.5	80.65	(Moazeni et al., 2017)
	Magnetite loaded on silica (Fe ₃ O ₄ /SiO ₂)	Time = 30 min Initial pH = 4.8 Dose = 1 g L ⁻¹ Conc. = 100 mg L ⁻¹	65	25.3	(Mahmoud et al., 2019)
	Wheat straw (WS-CK)	Time = 48 h Initial pH = 5 Dose = 0.2 g L ⁻¹ Conc. = 100 mg L ⁻¹	27.28	46.33	(Cao et al., 2019)
	Polypyrrole-based activated carbon (PPyAC4)	Time = 4 h Initial pH = 5 Dose = 5 g L ⁻¹ Conc. = 10 mg L ⁻¹	81.8	50	(Alghamdi et al., 2019)
	Magnetic chitosan/anaerobic granular sludge composite (M-CS-AnGS)	Time = 300 min Initial pH = 6 Dose = 0.8 g L ⁻¹ Conc. = 40 mg L ⁻¹	79.76	97.97	(Liu et al., 2017)
	Nano- <i>Oryza sativa</i> husk (OSH)	Time = 70 min Initial pH = 8 Dose = 12 g L ⁻¹ Conc. = 30 mg L ⁻¹	83	6.101	(Kaur et al., 2020)
	Natural clay	Time = 180 min Dose = 10 g L ⁻¹ Conc. = 20 mg L ⁻¹	65	25.07	(Kushwaha et al., 2020)
	Humic acid	Time = 180 min Dose = 10 g L ⁻¹ Conc. = 20 mg L ⁻¹	47.7	19.16	(Kushwaha et al., 2020)
	Modified walnut shell (WNS)	Time = 120 min Initial pH = 7 Dose = 2 g L ⁻¹ Conc. = 56.91 mg L ⁻¹	65	28.10	(Liu et al., 2019)
	Zeolite-supported nanoscale zero-valent iron (Z-NZVI)	Time = 10 h Initial pH = 6 Dose = 0.5 g L ⁻¹ Conc. = 60 mg L ⁻¹	75	85.37	(Li et al., 2018)

and 3.9 times than goethite-activated carbon composite (Adebayo et al., 2020) and nano-scaled zero-valent iron-supported zeolite composites (Chen et al., 2018), respectively. In addition, it possesses 15.12 times better adsorption capacity than magnetic graphene oxide functionalized tryptophan

(MGO-Trp) (Mahmoud et al., 2020), 4.7 times better than magnetite loaded on silica (Fe₃O₄/SiO₂) (Mahmoud et al., 2019), 3.95 times higher than tetraethyl orthosilicate superparamagnetic iron oxide (Gallo-Cordova et al., 2019), and 1.4 times higher than zeolite-supported nanoscale zero-valent

Table 5 Performance comparison of Cr (VI) adsorption on the synthesized nano-SiO₂ and various nano-adsorbents documented in the literature

Pollutant	Adsorbent	Optimum adsorption condition	Maximum removal efficiency (%)	Maximum adsorption capacity (mg g ⁻¹)	Reference
Cr (VI)	Nano-silica oxide	Time = 90 min Initial pH = 2 Dose = 1 g L ⁻¹ Conc. = 10 mg L ⁻¹	78.5	51.42	Present study
	As-synthesized MIP-202 MOF	Time = 30 min Initial pH = 7 Dose = 2 g L ⁻¹ Conc. = 50 mg L ⁻¹	52.6	19.01	(Diab et al., 2021)
	Aluminum–lanthanum mixed oxyhydroxide (ALMOH)	Time = 30 min Initial pH = 4.5 Dose = 2 g L ⁻¹ Conc. = 200 mg L ⁻¹	51	49.8	(Preethi et al., 2017)
	Tetraethyl orthosilicate superparamagnetic iron oxide (TEOS@MNP)	Time = 60 min Initial pH = 2.5 Dose = 0.3 g L ⁻¹ Conc. = 54 mg L ⁻¹	60	13	(Gallo-Cordova et al., 2019)
	(3-aminopropyl) tri-ethoxysilane superparamagnetic iron oxide (APTES@TEOS@MNP)	Time = 60 min Initial pH = 2.5 Dose = 0.3 g L ⁻¹ Conc. = 75 mg L ⁻¹	60	35	(Gallo-Cordova et al., 2019)
	Magnetite (Fe ₃ O ₄)	Time = 60 min Initial pH = 2 Dose = 5 g L ⁻¹ Conc. = 50 mg L ⁻¹	58.5	5.5	(Jain et al., 2018)
	Magnetic graphene oxide functionalized tryptophan (MGO-Trp)	Time = 25 min Initial pH = 2 Dose = 50 mg L ⁻¹ Conc. = 5 mg L ⁻¹	55	3.4	(Mahmoud et al., 2020)
	Goethite-activated carbon composite (GAC)	Time = 90 min Initial pH = 3 Dose = 20 mg L ⁻¹ Conc. = 400 mg L ⁻¹	34	6.4	(Adebayo et al., 2020)
	Nano-scaled zero-valent iron-supported zeolite composites (MCM-41)	Time = 80 min Initial pH = 5.7 Conc. = 50 mg L ⁻¹	20	19.5	(Chen et al., 2018)
	Molybdenum disulfide coated Mg/Al layered double hydroxide composites (LDHs@MoS ₂)	Time = 24 h Initial pH = 5 Dose = 0.5 g L ⁻¹ Conc. = 30 mg L ⁻¹	50.6	47	(Wang et al., 2017)
	Graphene oxide (GO)	Time = 120 min Initial pH = 3 Dose = 0.1 g L ⁻¹ Conc. = 200 mg L ⁻¹	66.2	49	(Shaban et al., 2018)

iron (Z-NZVI) (Li et al., 2018). Consequently, the fabricated nano-SiO₂ can be introduced as an appropriate and promising material for heavy metal removal from polluted water.

4 Conclusions

The purpose of this study was to examine the feasibility of removing Pb (II) and Cr (VI) from aqueous

solutions using silica oxide nanoparticles (nano-SiO₂). Consequently, firstly, nano-SiO₂ was successfully prepared, characterized, and used for Pb (II) and Cr (VI) removal from aqueous solutions using batch adsorption experiments. Secondly, the main operational conditions were investigated, and the findings showed that increasing contact time, adsorbent dosage, and temperature improved the removal efficiency of heavy metals. However, the increase in initial metal concentration had a negative effect on the treatment process. The optimal nano-SiO₂ dose for the removal of Pb (II) and Cr (VI) was determined to be 0.5 and 1 g L⁻¹, respectively. These dosages resulted in clearance efficiencies for Pb (II) and Cr (VI) of 82.29% and 78.5%, after 60 and 90 min, at initial pH of 5 and 2, using 10 mg L⁻¹ initial metal concentration, and at room temperature. The equilibrium isotherm model's applicability of Pb (II) and Cr (VI) adsorption process obeys the order of Freundlich > Langmuir > Temkin and assumes multilayer adsorption on heterogeneous surfaces demonstrating the anticipated physical metal ion adsorption onto the fabricated nano-SiO₂. The kinetic investigation of the Pb (II) and Cr (VI) adsorption process onto nano-SiO₂ indicated that the adsorption kinetics may be represented by the pseudo-second-order model. The synthesized nano-SiO₂ was identified as an effective adsorbent for the removal of Pb (II) and Cr (VI) from aqueous solutions. Eventually, this study could be considered a useful reference for future studies/applications for heavy metal removal.

Acknowledgements This paper is upon work supported by Science, Technology & Innovation Funding Authority (STDF), under grant 46138. The authors acknowledge Aswan University and Environment and Natural Materials Research Institute (ENMRI), City of Scientific Research and Technological Applications (SRTA-City) for providing all the needed facilities to conduct this research.

Author Contribution All authors contributed and were involved in all stages, including the conceptualization of the idea, designing experiments, conducting measurements, and explanation of data. Synthesis and characterization of nano-silica oxide were performed by Eslam Salama. The experimental work was conducted by Soheair Naeem and Naira Meko. Naira Meko and Eslam Salama wrote the original draft text, prepared figures, analyzed and discussed the data, and gave explanations. All authors reviewed, edited, and approved the final manuscript.

Funding Open access funding provided by The Science, Technology & Innovation Funding Authority (STDF) in cooperation with The Egyptian Knowledge Bank (EKB).

Data Availability All data generated or analyzed during this study are included in this manuscript.

Declarations

Competing Interests The authors declare no competing interests.

Open Access This article is licensed under a Creative Commons Attribution 4.0 International License, which permits use, sharing, adaptation, distribution and reproduction in any medium or format, as long as you give appropriate credit to the original author(s) and the source, provide a link to the Creative Commons licence, and indicate if changes were made. The images or other third party material in this article are included in the article's Creative Commons licence, unless indicated otherwise in a credit line to the material. If material is not included in the article's Creative Commons licence and your intended use is not permitted by statutory regulation or exceeds the permitted use, you will need to obtain permission directly from the copyright holder. To view a copy of this licence, visit <http://creativecommons.org/licenses/by/4.0/>.

References

- Adebayo, G. B., Adegoke, H. I., & Fauzeeyat, S. (2020). Adsorption of Cr(VI) ions onto goethite, activated carbon and their composite: Kinetic and thermodynamic studies. *Applied Water Science*, 10(9), 1–18. <https://doi.org/10.1007/S13201-020-01295-Z/FIGURES/17>. Springer Science and Business Media Deutschland GmbH.
- Afanador-Delgado, S. M., et al. (2022). Synthesis of SiO₂ nanoparticles assisted by thermocavitation in natural dye (Hibiscus sabdariffa L.). *Optics & Laser Technology*, 147, 107559. <https://doi.org/10.1016/J.OPTLASTEC.2021.107559>. Elsevier.
- Al Tbeishat, H. (2022). Novel in silico mRNA vaccine design exploiting proteins of M. tuberculosis that modulates host immune responses by inducing epigenetic modifications. *NatSR*, 12(1), 4645. <https://doi.org/10.1038/S41598-022-08506-4>. Nature Research.
- Ali, A. A., Ahmed, I. S., & Elfiky, E. M. (2021). Auto-combustion synthesis and characterization of iron oxide nanoparticles (α-Fe₂O₃) for removal of lead ions from aqueous solution. *Journal of Inorganic and Organometallic Polymers and Materials*, 31(1), 384–396. Springer.
- Alterary, S. S., Alshahrani, A. A., & Alsahli, S. A. (2022). Fabrication of novel buckypaper metal oxide nano-catalysis glycerol carbonate/MWCNTs membrane for efficient removal of heavy metals. *Heliyon*, 8(12), e12633. <https://doi.org/10.1016/J.HELİYON.2022.E12633>. Elsevier.

- Alghamdi, A. A., Al-Odayni, A. B., Saeed, W. S., Al-Kahtani, A., Alharthi, F. A., & Aouak, T. (2019). Efficient Adsorption of Lead (II) from Aqueous Phase Solutions Using Polypyrrole-Based Activated Carbon. *Materials*, *12*(12), 2020.
- Ambaye, T. G., et al. (2020). Mechanisms and adsorption capacities of biochar for the removal of organic and inorganic pollutants from industrial wastewater. *International Journal of Environmental Science and Technology*, *18*(10), 3273–3294. <https://doi.org/10.1007/S13762-020-03060-W>. Springer.
- Ammar, N. S., et al. (2021). Micro-mesoporous modified activated carbon from corn husks for removal of hexavalent chromium ions. *Applied Water Science*, *11*(9), 1–12. <https://doi.org/10.1007/S13201-021-01487-1/FIGURES/11>. Springer Science and Business Media Deutschland GmbH.
- Anjum, A., et al. (2023). A review of novel green adsorbents as a sustainable alternative for the remediation of chromium (VI) from water environments. *Heliyon*, *9*(5), e15575. <https://doi.org/10.1016/J.HELIYON.2023.E15575>. Elsevier.
- Aragaw, T. A., & Ayalew, A. A. (2023). Application of metal-based nanoparticles for metal removal for treatments of wastewater – A review. *Emerging Techniques for Treatment of Toxic Metals from Wastewater, 2023*, 183–231. <https://doi.org/10.1016/B978-0-12-822880-7.00001-7>. Elsevier.
- Bashir, A., et al. (2021). Magnetically recyclable L-cysteine capped Fe₃O₄ nanoadsorbent: A promising pH guided removal of Pb(II), Zn(II) and HCrO₄⁻ contaminants. *Journal of Environmental Chemical Engineering*, *9*(5), 105880. <https://doi.org/10.1016/J.JECE.2021.105880>. Elsevier.
- Blanchard, G., Maunay, M., & Martin, G. (1984). Removal of heavy metals from waters by means of natural zeolites. *Water Research*, *18*(12), 1501–1507. [https://doi.org/10.1016/0043-1354\(84\)90124-6](https://doi.org/10.1016/0043-1354(84)90124-6). Pergamon.
- Cao, Y., et al. (2019). Carbonization and ball milling on the enhancement of Pb(II) adsorption by wheat straw: Competitive effects of ion exchange and precipitation. *Bioresource Technology*, *273*, 70–76. <https://doi.org/10.1016/J.BIORTECH.2018.10.065>. Elsevier.
- Cataldo, S., et al. (2016). Pb(II) adsorption by a novel activated carbon – alginate composite material. A kinetic and equilibrium study. *International Journal of Biological Macromolecules*, *92*, 769–778. <https://doi.org/10.1016/j.ijbiomac.2016.07.099>. Elsevier B.V.
- Chen, Z., et al. (2018). Macroscopic and microscopic investigation of Cr(VI) immobilization by nanoscaled zero-valent iron supported zeolite MCM-41 via batch, visual, XPS and EXAFS techniques. *Journal of Cleaner Production*, *181*, 745–752. <https://doi.org/10.1016/J.JCLEPRO.2018.01.231>. Elsevier.
- Deravanesian, M., Beheshti, M., & Malekpour, A. (2015). The removal of Cr (III) and Co (II) ions from aqueous solution by two mechanisms using a new sorbent (alumina nanoparticles immobilized zeolite) — Equilibrium, kinetic and thermodynamic studies. *Journal of Molecular Liquids*, *209*, 246–257. <https://doi.org/10.1016/J.MOLLIQ.2015.05.038>. Elsevier.
- Diab, K. E., et al. (2021). Biocompatible MIP-202 Zr-MOF tunable sorbent for cost-effective decontamination of anionic and cationic pollutants from waste solutions. *Scientific Reports*, *11*(1), 6619. <https://doi.org/10.1038/S41598-021-86140-2>. Nature Publishing Group.
- Dubey, R. S., Rajesh, Y. B. R. D., & More, M. A. (2015). Synthesis and characterization of SiO₂ nanoparticles via sol-gel method for industrial applications. *Materials Today: Proceedings*, *2*(4–5), 3575–3579. <https://doi.org/10.1016/J.MATPR.2015.07.098>. Elsevier.
- Elkady, M. F., El-Aassar, M. R., & Hassan, H. S. (2016a). Adsorption profile of basic dye onto novel fabricated carboxylated functionalized co-polymer nanofibers. *Polymers*, *8*(5), 177. <https://doi.org/10.3390/POLYM8050177>. Multidisciplinary Digital Publishing Institute.
- Elkady, M. F., Shokry Hassan, H., & Salama, E. (2016b). Sorption profile of phosphorus ions onto ZnO nanorods synthesized via sonic technique. *Journal of Engineering (United Kingdom)*. <https://doi.org/10.1155/2016/2308560>. Hindawi Limited.
- Elkady, M. F., et al. (2017). Novel magnetic zinc oxide nanotubes for phenol adsorption: Mechanism modeling. *Materials*, *10*(12), 1355. <https://doi.org/10.3390/MA10121355>. Multidisciplinary Digital Publishing Institute.
- Elkady, M., et al. (2020). Novel eco-friendly electrospun nanomagnetic zinc oxide hybridized PVA/alginate/chitosan nanofibers for enhanced phenol decontamination. *Environmental Science and Pollution Research*, *27*(34), 43077–43092. <https://doi.org/10.1007/S11356-020-10247-8/FIGURES/14>. Springer Science and Business Media Deutschland GmbH.
- Esfandiari, N., Suri, R., & McKenzie, E. R. (2022). Competitive sorption of Cd, Cr, Cu, Ni, Pb and Zn from stormwater runoff by five low-cost sorbents; effects of co-contaminants, humic acid, salinity and pH. *Journal of Hazardous Materials*, *423*, 126938. <https://doi.org/10.1016/J.JHAZMAT.2021.126938>. Elsevier.
- Fathy, N. A., El-Khouly, S. M., & El-Shafey, O. I. (2020). Modified carbon nanostructures obtained from sugarcane bagasse hydrochar for treating chromium-polluted water. *Current Analytical Chemistry*, *17*(7), 975–988. <https://doi.org/10.2174/1573411016666200106101921>. Bentham Science Publishers.
- Freundlich, H. M. F. (1906). Over the adsorption in solution. *The Journal of Physical Chemistry*, *57*(385471), 1100–1107.
- Gallo-Cordova, A., del Puerto Morales, M., & Mazarío, E. (2019). Effect of the surface charge on the adsorption capacity of chromium(VI) of iron oxide magnetic nanoparticles prepared by microwave-assisted synthesis. *Water*, *11*(11), 2372. <https://doi.org/10.3390/W11112372>. Multidisciplinary Digital Publishing Institute.
- Godini, K., et al. (2020). Application of ZnO nanorods doped with Cu for enhanced sonocatalytic removal of Cr (VI) from aqueous solutions. *Environmental Science and Pollution Research*, *27*(3), 2691–2706. Springer.
- Gouamid, M., Ouahrani, M. R., & Bensaci, M. B. (2013). Adsorption equilibrium, kinetics and thermodynamics of methylene blue from aqueous solutions using date palm leaves. *Energy Procedia*, *36*, 898–907. <https://doi.org/10.1016/J.EGYPRO.2013.07.103>. Elsevier.
- Goyne, K. W., et al. (2002). Surface charge of variable porosity Al₂O₃(s) and SiO₂(s) adsorbents. *Journal of Porous*

- Materials*, 9(4), 243–256. <https://doi.org/10.1023/A:1021631827398/METRICS>. Springer.
- Hasanzadeh, R., et al. (2017). Effective removal of toxic metal ions from aqueous solutions: 2-bifunctional magnetic nanocomposite base on novel reactive PGMA-MAN copolymer@Fe₃O₄ nanoparticles. *Journal of Colloid and Interface Science*, 490, 727–746. <https://doi.org/10.1016/j.jcis.2016.11.098>. Academic Press Inc.
- Hassan, H. S., et al. (2017). Fabrication of novel magnetic zinc oxide cellulose acetate hybrid nano-fiber to be utilized for phenol decontamination. *Journal of the Taiwan Institute of Chemical Engineers*, 78, 307–316. <https://doi.org/10.1016/J.JTICE.2017.06.021>. Elsevier.
- Hosseini, R., Sayadi, M. H., & Shekari, H. (2019). Adsorption of nickel and chromium from aqueous solutions using copper oxide nanoparticles: Adsorption isotherms, kinetic modeling, and thermodynamic studies. *Avicenna Journal of Environmental Health Engineering*, 6(2), 66–74. Hamadan University of Medical Sciences.
- Iconaru, S. L., et al. (2016). Magnetite (Fe₃O₄) nanoparticles as adsorbents for As and Cu removal. *Applied Clay Science*, 134, 128–135. <https://doi.org/10.1016/j.clay.2016.08.019>. Elsevier Ltd.
- Jain, M., et al. (2018). Development of iron oxide/activated carbon nanoparticle composite for the removal of Cr (VI), Cu (II) and Cd (II) ions from aqueous solution. *Water Resources and Industry*, 20, 54–74. Elsevier.
- Karami, H. (2013). Heavy metal removal from water by magnetite nanorods. *Chemical Engineering Journal*, 219, 209–216. <https://doi.org/10.1016/j.cej.2013.01.022>. Elsevier.
- Kaur, M., Kumari, S., & Sharma, P. (2020). Removal of Pb (II) from aqueous solution using nano-adsorbent of *Oryza sativa* husk: Isotherm, kinetic and thermodynamic studies. *Biotechnology Reports*, 25, e00410.
- Kim, E. J., et al. (2013). Hierarchically structured manganese oxide-coated magnetic nanocomposites for the efficient removal of heavy metal ions from aqueous systems. *ACS Applied Materials and Interfaces*, 5(19), 9628–9634. https://doi.org/10.1021/AM402615M/SUPPL_FILE/AM402615M_SI_001.PDF. American Chemical Society.
- Kotsyuda, S. S., et al. (2017). Bifunctional silica nanospheres with 3-aminopropyl and phenyl groups. Synthesis approach and prospects of their applications. *Applied Surface Science*, 420, 782–791. <https://doi.org/10.1016/j.apsusc.2017.05.150>. Elsevier B.V.
- Kuang, Y., Zhang, X., & Zhou, S. (2020). Adsorption of methylene blue in water onto activated carbon by surfactant modification. *Water*, 12(2), 587. <https://doi.org/10.3390/W12020587>. Multidisciplinary Digital Publishing Institute.
- Kumar, J. A., et al. (2022). Effect of Ca²⁺ ions on naphthalene adsorption/desorption onto calcium oxide nanoparticle: Adsorption isotherm, kinetics and regeneration studies. *Environmental Research*, 204, 112070. <https://doi.org/10.1016/J.ENVRES.2021.112070>. Academic Press.
- Kushwaha, A., Rani, R., & Patra, J. K. (2020). Adsorption kinetics and molecular interactions of lead [Pb(II)] with natural clay and humic acid. *International Journal of Environmental Science and Technology*, 17(3), 1325–1336. <https://doi.org/10.1007/S13762-019-02411-6/FIGURES/5>. Springer.
- Lagergren, S. (1898). About the theory of so-called adsorption of soluble substances. *Sven. Vetenskapsakad. Handlingar*, 24(6), 1–39. <https://doi.org/10.1252/JCEJ.38.402>
- Langmuir, I. (1916). The constitution and fundamental properties of solids and liquids. Part I. Solids. *Journal of the American Chemical Society*, 38(11), 2221–2295. https://doi.org/10.1021/JA02268A002/ASSET/JA02268A002.FP.PNG_V03. American Chemical Society.
- Largitte, L., & Pasquier, R. (2016). A review of the kinetics adsorption models and their application to the adsorption of lead by an activated carbon. *Chemical Engineering Research and Design*, 109, 495–504. <https://doi.org/10.1016/J.CHERD.2016.02.006>. Elsevier.
- Li, Z., et al. (2018). Zeolite-supported nanoscale zero-valent iron: New findings on simultaneous adsorption of Cd(II), Pb(II), and As(III) in aqueous solution and soil. *Journal of Hazardous Materials*, 344, 1–11. <https://doi.org/10.1016/J.JHAZMAT.2017.09.036>. Elsevier.
- Li, Y., et al. (2019). Super rapid removal of copper, cadmium and lead ions from water by NTA-silica gel. *RSC Advances*, 9(1), 397–407. <https://doi.org/10.1039/C8RA08638A>. Royal Society of Chemistry.
- Liu, G., Zhang, W., & Luo, R. (2019). Synthesis, characterization of amino-modified walnut shell and adsorption for Pb(II) ions from aqueous solution. *Polymer Bulletin*, 76(3), 1099–1114.
- Liu, T. (2017). Magnetic chitosan/anaerobic granular sludge composite: Synthesis, characterization and application in heavy metal ions removal. *Journal of Colloid and Interface Science*, 508, 405–414.
- Lord, F. M., & Kittelberger, J. S. (1974). On the determination of activation energies in thermal desorption experiments. *Surface Science*, 43(1), 173–182. [https://doi.org/10.1016/0039-6028\(74\)90226-X](https://doi.org/10.1016/0039-6028(74)90226-X). North-Holland.
- Mahmoud, M. E., & Al-Bishri, H. M. (2011). Supported hydrophobic ionic liquid on nano-silica for adsorption of lead. *Chemical Engineering Journal*, 166(1), 157–167. <https://doi.org/10.1016/J.CEJ.2010.10.046>. Elsevier.
- Mahmoud, M. E., et al. (2019). Green nanosilica@folic Acid (VB9) nanocomposite for engineered adsorptive water remediation of bivalent lead, cadmium and copper. *Powder Technology*, 344, 719–729. <https://doi.org/10.1016/J.POWTEC.2018.12.055>. Elsevier.
- Mahmoud, M. E., et al. (2020). Microwave-assisted adsorption of Cr(VI), Cd(II) and Pb(II) in presence of magnetic graphene oxide-covalently functionalized-tryptophan nanocomposite. *Journal of Alloys and Compounds*, 823, 153855. <https://doi.org/10.1016/J.JALLCOM.2020.153855>. Elsevier.
- Maryam, S., & Gul, A. (2023). Heavy metal remediation by nanotechnology. In *Phytoremediation*. Springer, pp. 571–597. https://doi.org/10.1007/978-3-031-17988-4_26
- Mehdinia, A., Mollazadeh-Moghaddam, A., & Jabbari, A. (2021). Fabrication of silver–2-aminoterephthalic acid coordination polymer-coated Fe₃O₄ for effective removal of lead from aqueous media. *International Journal of Environmental Research*, 15(4), 631–644. <https://doi.org/10.1007/S41742-021-00339-9/TABLES/5>. Springer Science and Business Media Deutschland GmbH.

- Moazeni, M., Ebrahimi, A., Rafiei, N., & Pourzamani, H. R. (2017). Removal of Lead Ions from Aqueous Solution by Nano Zero-Valent Iron (nZVI). *Health Scope*, 6(2), 40240.
- Najafi, M., Yousefi, Y., & Rafati, A. A. (2012). Synthesis, characterization and adsorption studies of several heavy metal ions on amino-functionalized silica nano hollow sphere and silica gel. *Separation and Purification Technology*, 85, 193–205. <https://doi.org/10.1016/J.SEPPUR.2011.10.011>. Elsevier.
- Pearson, R. G. (1968). Hard and soft acids and bases, HSAB, part I: Fundamental principles. *Journal of Chemical Education*, 45(9), 581. <https://doi.org/10.1021/ED045P581>. Division of Chemical Education.
- Rahbari, M., & Goharizi, A. S. (2009). Adsorption of lead(II) from water by carbon nanotubes: Equilibrium, kinetics, and thermodynamics. *Water Environment Research*, 81(6), 598–607. <https://doi.org/10.2175/106143008X370511>. John Wiley & Sons Ltd.
- Preethi, J., Prabhu, S. M., & Meenakshi, S. (2017). Effective adsorption of hexavalent chromium using biopolymer assisted oxyhydroxide materials from aqueous solution. *Reactive and Functional Polymers*, 117, 16–24.
- Rahmani, A. R., et al. (2011). Synthesis of zero valent iron nanoparticles (nzvi) and its efficiency in arsenic removal from aqueous solutions. *Water Wastewater*, 1, 35–41.
- Saad, A. M., et al. (2022). Impact of green chitosan nanoparticles fabricated from shrimp processing waste as a source of nano nitrogen fertilizers on the yield quantity and quality of wheat (*Triticum aestivum* L.) cultivars. *Molecules*, 27(17), 5640. <https://doi.org/10.3390/MOLECULES27175640/S1>. MDPI.
- Salama, E., Hamdy, A., et al. (2022a). Evaluation of Zn adenine-based bio-MOF for efficient remediation of different types of dyes. *Adsorption Science and Technology*. <https://doi.org/10.1155/2022/6818348>. Hindawi Limited.
- Salama, E., Ghanim, M., et al. (2022b). Novel aspartic-based bio-MOF adsorbent for effective anionic dye decontamination from polluted water. *RSC Advances*, 12(29), 18363–18372. <https://doi.org/10.1039/D2RA02333D>. Royal Society of Chemistry.
- Salama, E., Samy, M., et al. (2022c). The superior performance of silica gel supported nano zero-valent iron for simultaneous removal of Cr (VI). *Scientific Reports*, 12(1), 1–19. <https://doi.org/10.1038/s41598-022-26612-1>. Nature Publishing Group.
- Salama, E., Hassan, H. S., & Elkady, M. F. (2015). Adsorption behavior of organic pollutant from aqueous solution onto synthesized zinc oxide nanotubes: Equilibrium, kinetic and thermodynamic investigation. *office@multidisciplinarywulfenia.org*, 22(1). <https://www.researchgate.net/publication/289229734>. Accessed: 13 Dec 2021.
- Samrot, A. V., et al. (2019). Surface-engineered super-paramagnetic iron oxide nanoparticles for chromium removal. *International Journal of Nanomedicine*, 14, 8105. Dove Press.
- Samy, M., et al. (2023). Heterogeneous activation of persulfate by a novel nano-magnetite/ZnO/activated carbon nano-hybrid for carbofuran degradation: Toxicity assessment, water matrices, degradation mechanism and radical and non-radical pathways. *Process Safety and Environmental Protection*, 169, 337–351. <https://doi.org/10.1016/J.PSEP.2022.11.038>. Elsevier.
- Santhosh, C., et al. (2016). Role of nanomaterials in water treatment applications: A review. *Chemical Engineering Journal*, 306, 1116–1137. <https://doi.org/10.1016/J.CEJ.2016.08.053>. Elsevier.
- Shahbazi, A., Younesi, H., & Badieli, A. (2012). Synthesis of organic-inorganic hybrid amine based on nanostructured silicate materials and its application for removal of heavy metal ions from aqueous solution. *Journal of Water and Wastewater; Ab va Fazilab (in persian)*, 23(4), 13–21. Water and Wastewater Consulting Engineers.
- Shaban, M., Abukhadra, M. R., Rabia, M., Elkader, Y. A., & Abd El-Halim, M. R. (2018). Investigation the adsorption properties of graphene oxide and polyaniline nano/micro structures for efficient removal of toxic Cr(VI) contaminants from aqueous solutions; kinetic and equilibrium studies,. *Rendiconti Lincei. Scienze Fisiche e Naturali*, 29(1), 141–154.
- Sharma, P., et al. (2022). Surface functionalization of bamboo leave mediated synthesized SiO₂ nanoparticles: Study of adsorption mechanism, isotherms and enhanced adsorption capacity for removal of Cr (VI) from aqueous solution. *Environmental Research*, 214, 113761. <https://doi.org/10.1016/J.ENVRES.2022.113761>. Academic Press.
- Shen, H., et al. (2013). New insights into the sorption and detoxification of chromium(VI) by tetraethylenepentamine functionalized nanosized magnetic polymer adsorbents: Mechanism and pH effect. *Industrial and Engineering Chemistry Research*, 52(36), 12723–12732. https://doi.org/10.1021/IE4010805/SUPPL_FILE/IE4010805_SI_001.PDF. American Chemical Society.
- Shokry, H., Elkady, M., & Salama, E. (2020). Eco-friendly magnetic activated carbon nano-hybrid for facile oil spills separation. *Scientific Reports*, 10(1), 1–17. <https://doi.org/10.1038/s41598-020-67231-y>. Nature Publishing Group.
- Shokry Hassan, H. (2019). Role of preparation technique in the morphological structures of innovative nano-cation exchange. *Journal of Materials Research and Technology*, 8(3), 2854–2864. <https://doi.org/10.1016/J.JMRT.2019.04.023>. Elsevier.
- Soon, W. L., et al. (2022). Plant-based amyloids from food waste for removal of heavy metals from contaminated water. *Chemical Engineering Journal*, 445, 136513. <https://doi.org/10.1016/J.CEJ.2022.136513>. Elsevier.
- Tan, Y., Chen, M., & Hao, Y. (2012). ‘High efficient removal of Pb (II) by amino-functionalized Fe₃O₄ magnetic nanoparticles. *Chemical Engineering Journal*, 191, 104–111. <https://doi.org/10.1016/J.CEJ.2012.02.075>. Elsevier.
- Temkin, M. I. (1940). Kinetics of ammonia synthesis on promoted iron catalysts. *Acta Physiochim* 12, 327–356. <https://cir.nii.ac.jp/crid/1573387451182255872>. Accessed: 28 Oct 2023. URSS.
- Thinakaran, N., et al. (2008). Removal of Acid Violet 17 from aqueous solutions by adsorption onto activated carbon prepared from sunflower seed hull. *Journal of Hazardous Materials*, 151(2–3), 316–322. <https://doi.org/10.1016/J.JHAZMAT.2007.05.076>. Elsevier.
- Tu, Y. J., et al. (2017). Efficient removal/recovery of Pb onto environmentally friendly fabricated copper ferrite nanoparticles. *Journal of the Taiwan Institute of Chemical*

- Engineers*, 71, 197–205. <https://doi.org/10.1016/j.jtice.2016.12.006>. Taiwan Institute of Chemical Engineers.
- Üner, O., Geçgel, Ü., & Bayrak, Y. (2016). Adsorption of methylene blue by an efficient activated carbon prepared from *Citrullus lanatus* rind: Kinetic, isotherm, thermodynamic, and mechanism analysis. *Water, Air, and Soil Pollution*, 227(7), 1–15. <https://doi.org/10.1007/S11270-016-2949-1/TABLES/8>. Springer International Publishing.
- Verma, M., et al. (2017a). Adsorptive removal of Pb (II) ions from aqueous solution using CuO nanoparticles synthesized by sputtering method. *Journal of Molecular Liquids*, 225, 936–944. <https://doi.org/10.1016/j.molliq.2016.04.045>. Elsevier B.V.
- Verma, R., et al. (2017b). Novel glycine-functionalized magnetic nanoparticles entrapped calcium alginate beads for effective removal of lead. *Microchemical Journal*, 130, 168–178. <https://doi.org/10.1016/j.microc.2016.08.006>. Elsevier Inc.
- Vikrant, K., et al. (2017). Metal–organic frameworks (MOFs): Potential and challenges for capture and abatement of ammonia. *Journal of Materials Chemistry A*, 5(44), 22877–22896. <https://doi.org/10.1039/C7TA07847A>. Royal Society of Chemistry.
- Wadhawan, S., et al. (2020). Role of nanomaterials as adsorbents in heavy metal ion removal from waste water: A review. *Journal of Water Process Engineering*, 33, 101038. <https://doi.org/10.1016/j.jwpe.2019.101038>. Elsevier Ltd.
- Walker, J. (1913). Van't Hoff memorial lecture. *Journal of the Chemical Society, Transactions*, 103(0), 1127–1143. <https://doi.org/10.1039/CT9130301127>. The Royal Society of Chemistry.
- Wang, J., et al. (2017). Preparation of Molybdenum Disulfide Coated Mg/Al Layered Double Hydroxide Composites for Efficient Removal of Chromium(VI). *ACS Sustainable Chemistry & Engineering*, 5(8), 7165–7174.
- Weber, W. J., Jr., & Morris, J. C. (1963). Kinetics of adsorption on carbon from solution. *Journal of the Sanitary Engineering Division*, 89(2), 31–59. <https://doi.org/10.1061/JSEDA1.0000430>. American Society of Civil Engineers.
- Wen, J., et al. (2022). Pyrogallol acid modified nanoscale zero-valent iron efficiently removed Cr(VI) by improving adsorption and electron selectivity. *Chemical Engineering Journal*, 443, 136510. <https://doi.org/10.1016/J.CEJ.2022.136510>. Elsevier.
- Xiao, Z., et al. (2017). Ultra-efficient removal of chromium from aqueous medium by biogenic iron based nanoparticles. *Separation and Purification Technology*, 174, 466–473. <https://doi.org/10.1016/J.SEPPUR.2016.10.047>. Elsevier.
- Xiong, C., et al. (2019). Selective adsorption of Pb(II) from aqueous solution using nanosilica functionalized with diethanolamine: Equilibrium, kinetic and thermodynamic. *Microchemical Journal*, 146, 270–278. <https://doi.org/10.1016/J.MICROC.2019.01.005>. Elsevier.
- Xu, D., et al. (2015). Poly(ethylene-co-vinyl alcohol) functional nanofiber membranes for the removal of Cr(VI) from water. *Industrial and Engineering Chemistry Research*, 54(27), 6836–6844. https://doi.org/10.1021/ACS.IECR.5B00995/SUPPL_FILE/IE5B00995_SI_001.PDF. American Chemical Society.
- Xu, P., et al. (2006). Preparation and morphology of SiO₂/PMMA nanohybrids by microemulsion polymerization. *Colloid and Polymer Science*, 284(7), 755–762. <https://doi.org/10.1007/S00396-005-1428-9/FIGURES/6>. Springer.
- Yuan, X., et al. (2018). Hierarchically porous nitrogen-doped carbon materials as efficient adsorbents for removal of heavy metal ions. *Process Safety and Environmental Protection*, 119, 320–329. <https://doi.org/10.1016/J.PSEP.2018.08.012>. Elsevier.
- Zhang, X., et al. (2022). Outstanding performance of sulfurated titanomagemite (Fe₂TiO₅) for hexavalent chromium removal: Sulfuration promotion mechanism and its application in chromium resource recovery. *Chemosphere*, 287. <https://doi.org/10.1016/J.CHEMOSPHERE.2021.132360>. Elsevier Ltd.
- Zhu, K., et al. (2017). Efficient removal of Pb(II) from aqueous solution by modified montmorillonite/carbon composite: Equilibrium, kinetics, and thermodynamics. *Journal of Chemical and Engineering Data*, 62(1), 333–340. https://doi.org/10.1021/ACS.JCED.6B00676/SUPPL_FILE/JE6B00676_SI_001.PDF. American Chemical Society.

Publisher's Note Springer Nature remains neutral with regard to jurisdictional claims in published maps and institutional affiliations.